



HAL
open science

The influence of the equation of state on the cellular structure of gaseous detonations

S. Taileb, J. Melguizo-Gavilanes, A. Chinnayya

► **To cite this version:**

S. Taileb, J. Melguizo-Gavilanes, A. Chinnayya. The influence of the equation of state on the cellular structure of gaseous detonations. *Physics of Fluids*, 2021, 33 (3), pp.036105. 10.1063/5.0040723 . hal-03412017

HAL Id: hal-03412017

<https://hal.science/hal-03412017>

Submitted on 10 Nov 2021

HAL is a multi-disciplinary open access archive for the deposit and dissemination of scientific research documents, whether they are published or not. The documents may come from teaching and research institutions in France or abroad, or from public or private research centers.

L'archive ouverte pluridisciplinaire **HAL**, est destinée au dépôt et à la diffusion de documents scientifiques de niveau recherche, publiés ou non, émanant des établissements d'enseignement et de recherche français ou étrangers, des laboratoires publics ou privés.

This is the author's peer reviewed, accepted manuscript. However, the online version of record will be different from this version once it has been copyedited and typeset.

PLEASE CITE THIS ARTICLE AS DOI: 10.1063/1.50040723

“EOS influence on gaseous detonations”

The influence of the Equation of State on the cellular structure of gaseous detonations

S. Taïleb,¹ J. Melguizo-Gavilanes,^{1, a)} and A. Chinnayya¹

*Institut Pprime, UPR 3346 CNRS, ISAE-ENSMA, Université de Poitiers,
86961 Futuroscope-Chasseneuil, France*

(Dated: January 12, 2021)

The propagation of multidimensional gaseous detonations at elevated pressures was investigated numerically. Initial conditions at which deviations from ideal gas are expected (i.e., $p_0 > 2$ MPa) were used to assess whether real gas effects influence their multi-cellular structure. The simplest equation of state that accounts for real gas effects was selected, *Noble-Abel*, and compared with results obtained using perfect gas. Approximate and exact relationships are provided for the von-Neumann and Chapman-Jouguet states, as well as sound speeds, for both equations of state. Results show that real gas effects alter the multi-cellular structure of gaseous detonations at elevated pressures. Moreover, neglecting these effects renders a more *irregular* structure than that obtained when real gas effects are reinstated. The source of the perceived instabilities was identified as a Mach bifurcation due to jetting and their growth was related to a shear layer triple point interaction, giving birth to new triple points. The more unstable structure seems to arise from an effective change in the isentropic coefficient that is not included in the perfect gas formulation.

Keywords: gaseous detonations, Noble-Abel EOS, cellular structure, high pressure, numerical simulation

^{a)}The authors to whom correspondence may be addressed: josue.melguizo-gavilanes@cnrs.pprime.fr, said.taïleb@ensma.fr

“EOS influence on gaseous detonations”

I. INTRODUCTION

Any gaseous combustible mixture exhibits two modes of combustion: deflagration and detonation. Their propagation mechanisms are fundamentally different. While in deflagrations chemical reactions are initiated due to heat and mass diffusion, in detonations chemistry is activated due to the adiabatic compression caused by the leading shock. A strong coupling between the leading shock and the reaction zone is a key feature of self-sustained detonation waves¹. Fundamental understanding of the latter regime of combustion is necessary to propulsion²⁻⁶ and industrial/nuclear safety⁷. Detonation quenching limits and re-initiation mechanisms for different fuel mixtures are experimentally characterized using their cellular structure; engineering correlations are oftentimes based on this metric. Indeed, detonations that exhibit *irregular* cellular patterns are harder to quench, and require lower reactive layer heights to propagate. Knowledge of the cellular structure is thus crucial for safe and optimal design.

Theoretical, experimental and numerical research on detonations have focused primarily on two regimes⁸: (i) condensed phase (solid/porous explosives, homogeneous/bubbly liquids) characterized by initial densities of $\rho_0 = 800 - 2000 \text{ kg/m}^3$, detonation velocities, $D = 6 - 9 \text{ km/s}$, and pressures in the product gases (Chapman-Jouguet state), $p_{CJ} \sim 10 \text{ GPa}$; and (ii) gases at near/sub-atmospheric conditions characterized by $\rho_0 = 0.1 - 1 \text{ kg/m}^3$, $D = 1 - 3 \text{ km/s}$, and $p_{CJ} \sim 1 \text{ MPa}$. In the range of $\rho_0 = 1 - 250 \text{ kg/m}^3$, namely gases at elevated pressures and intermediate densities, research is sparse. In the latter regime, real gas effects may play an important role. The main assumptions made in an ideal/perfect gas description of a fluid are that the molecules interact with their containers but not with each other; that the size of the molecules is neglected (sensible if the mean free path, ℓ , is large compared to molecular size, d - regime (ii)); and that the importance of intermolecular forces is minor, which decreases with increasing temperature. Including real gas effects in the modeling entails relaxing these assumptions. A typical example of an equation of state (EOS) for modeling real gases is *van der Waals*: $(p + a/v^2)(v - b) = RT$, where p is pressure, v specific volume, T is the temperature, and R is the specific gas constant; a and b are functions of the critical properties of the gas considered that account for intermolecular forces and the volume occupied by the molecules, respectively.

Neglecting the corrections to p and v (i.e., $a = b = 0$) reverts the above expression to the

This is the author's peer reviewed, accepted manuscript. However, the online version of record will be different from this version once it has been copyedited and typeset.

PLEASE CITE THIS ARTICLE AS DOI: 10.1063/1.50040723

“EOS influence on gaseous detonations”

ideal gas formulation, $pv = RT$. Real gas effects are significant at high p and low T , due to potential phase changes; at low p and high T , due to possible dissociation/ionization of the gas⁹, as well as at supercritical states.

In gaseous detonations, both pressure and temperature are high, with ratios across the front that can easily reach values of 50 and 15, respectively¹. For gases at initial pressures $p_0 \geq 0.1$ MPa and ambient temperature, $T_0 = 300$ K, the post-shock state enters a regime where the volume occupied by the molecules may need to be accounted for, but intermolecular forces should play a minor role due to the high temperatures in this region. The *Noble-Abel* EOS, $p(v - b) = RT$, accounts for this correction with the co-volume, b , being the only parameter in the formulation, taken to be independent of the critical state of the gas.

Experimental data on the structure of detonations in gaseous mixtures at initial pressures greater than $p_0 = 0.1$ MPa are limited. Classical experiments include those performed in the 1960's in which detonation velocities for $\text{H}_2\text{-O}_2$ at initial pressures $p_0 = 0.1 - 7$ MPa, and $X_{\text{H}_2, \text{vol}} = 40 - 80\%$ were reported¹⁰; spinning detonations and their stability up to $p_0 = 0.2$ MPa¹¹ and the application of optical reflectivity to unveil the detonation structure of oxygen-enriched H_2 detonations at $p_0 = 0.14 - 0.32$ MPa¹² were also topics of research during that decade. In the mid 1970's experimental evidence was gathered attesting to the fact that up to $p_0 = 1$ MPa, there is no qualitative change in the structure of gaseous detonations. This observation contradicted the notion that for increasing pressure the inhomogeneities of the front become less and less significant¹³. In the 1980's and early 1990's an extensive data base was collected for detonation velocities and cell sizes of hydrogen and hydrocarbon-oxygen-nitrogen mixtures for initial pressures up to 3 MPa and 40 MPa, respectively¹⁴⁻¹⁸.

In the mid 1980's, detonation parameters for $\text{H}_2\text{-O}_2$ and $\text{H}_2\text{-Air}$ mixtures at $T_0 = 80 - 1000$ K and $p_0 = 0.01 - 100$ MPa for $X_{\text{H}_2, \text{vol}} = 9.56 - 91\%$ were computed using *van der Waals* EOS¹⁹. The authors compared their results with predictions given by an ideal gas formulation; they concluded that non-idealities begin to occur around $p_0 = 1.2$ MPa and $T_0 = 300$ K. Additional work in 1995 by Schmitt and Butler⁸ identified the need to develop standard computational tools that would be applicable to gaseous systems at elevated initial pressures, namely implementing various cubic EOS (*van der Waals*, *Redlich-Kwong*, *Soave and Peng-Robinson*) with detailed kinetics to compute detonation parameters as well as the one-dimensional steady detonation structure (ZND). Their work showed that ideal gas

“EOS influence on gaseous detonations”

descriptions begin to become inaccurate for initial pressures as low as 1 MPa, and that cubic EOS more accurately describe the variation of detonation velocity as a function of initial pressure.

Furthermore, the influence of the repulsive part of the intermolecular potential on the thermodynamics of hot gases at high pressures was studied by Heuze²⁰. The author aimed to develop an EOS with a broad range of applicability, ranging from gases at low initial pressures to condensed explosives. It was emphasized that various equations of state leading to the same detonation velocity yield significantly different Chapman-Jouguet pressures and temperatures depending on the inter-molecular potential chosen, hence the need for accurate temperature measurements on the detonation products. Lastly, while not specific to detonations, there is recent work on inert compressible flow at high upstream pressures^{21–23}, and multi-phase, multi-component mixing at super-critical conditions^{24,25} where non-idealities are shown to play an important role; the practical implications of the latter research are related to safety hazards (i.e. storage, handling and use of liquid fuels). To the authors' knowledge, no work has been carried out addressing real gas effects on multidimensional gaseous detonations at elevated pressure. Therefore here, we investigate to what extent, if at all, the detonation cellular structure is affected by real gas effects. Two-dimensional unsteady detonations are computed using the perfect gas formulation and compared against results obtained using the *Noble-Abel* EOS.

This manuscript is organised as follows: the physical model is presented in Section II for both EOS. Section III describes the computational methodology used. Numerical results and discussion are included in Section IV. Finally, concluding remarks are given in Section V.

II. MATHEMATICAL MODEL

A. Governing equations and equations of state

The flow is described by the reactive Euler equations

$$\frac{\partial U}{\partial t} + \frac{\partial F(U)}{\partial x} + \frac{\partial G(U)}{\partial y} = S(U) \quad (1)$$

“EOS influence on gaseous detonations”

U , F , G , and S are the conserved variables, convective fluxes along the x and y directions, and the the source term vectors, respectively.

$$U = \begin{bmatrix} \rho \\ \rho u \\ \rho v \\ \rho e_t \\ \rho Y_f \end{bmatrix}, F = \begin{bmatrix} \rho u \\ \rho u^2 + p \\ \rho v u \\ (\rho e_t + p)u \\ \rho Y_f u \end{bmatrix}, G = \begin{bmatrix} \rho v \\ \rho u v \\ \rho v^2 + p \\ (\rho e_t + p)v \\ \rho Y_f v \end{bmatrix}, S = \begin{bmatrix} 0 \\ 0 \\ 0 \\ 0 \\ -\rho \dot{\omega} \end{bmatrix}$$

where ρ is the density, u, v are the horizontal and vertical velocity components, p is the pressure, e_t is the total energy, Y_f is the fuel mass fraction, and $\dot{\omega}$ is the fuel consumption rate; fresh gas is characterized by $Y_f = 1$, and burnt gas by $Y_f = 0$.

Energy conservation is solved in its total energy form with,

$$e_t = e(p, \rho) + \frac{u^2 + v^2}{2} - (1 - Y_f)q \quad (2)$$

where e is the internal energy and q the total energy content of the mixture. Two EOS are used: Perfect Gas (PG), $p v = RT$, and Noble-Abel (NA), $p(v - b) = RT$ where $R = R_u/W$ and W is the molecular weight of the mixture. The latter is the simplest correction to PG in which a co-volume, b , is introduced to account for the volume occupied by molecules present in the gas. Moreover, this EOS is convex²⁶⁻²⁸ which has advantages for its numerical implementation when using shock capturing schemes based on Riemann solvers.

The internal energy, e , and sound speed, c , for PG read:

$$e = \frac{p}{(\gamma - 1)\rho}; \quad c^2 = \frac{\gamma p}{\rho} \quad (3)$$

For NA, e and c are given by:

$$e = \frac{p}{(\gamma - 1)\rho}(1 - b\rho); \quad c^2 = \frac{\gamma p}{\rho}(1 - b\rho)^{-1} \quad (4)$$

In the expressions above, $\gamma = c_p/c_v$, is the ratio of specific heats, here, assumed to be constant. Extensions to multiphase and multispecies formulations can be found in recent work^{26,29,30}.

The chemistry is modeled using a one-step irreversible reaction, $\mathcal{R} \rightarrow \mathcal{P}$, following an Arrhenius rate law. The chemical source term is given by

$$\dot{\omega} = A_s Y_f \exp(-E_a/R_u T) \quad (5)$$

“EOS influence on gaseous detonations”

where A_s is the pre-exponential factor and E_a is the activation energy.

For single-step kinetics, the detonation cellular structure is known to depend on three main factors: q , γ and E_a (i.e. increasing E_a leads to more *irregular* structures). For detailed kinetics, Radulescu³¹ and Ng³² showed, based on the theoretical development of Short and Sharpe³³, that the ratio of the induction to the reaction lengths can be used to classify the regularity of the cellular structure of detonations.

B. Theoretical considerations

In this section, exact and approximate expressions for the Chapman-Jouguet (CJ) and von Neumann states (vN) are derived for NA by algebraically solving the system of Eqs. (6) following standard methodologies described in detonation theory textbooks such as Fickett and Davis¹ (see Appendix 2A). These expressions will serve later in the study to understand the main differences between the EOS considered.

1. Chapman-Jouguet state

The Rankine-Hugoniot jump conditions for mass, momentum and energy, in a wave attached reference frame read:

$$\begin{aligned}\rho_1(D - u_1) &= \rho_0 D \\ \rho_1(D - u_1)^2 + p_1 &= \rho_0 D^2 + p_0 \\ e_1 + \frac{p_1}{\rho_1} + \frac{(D - u_1)^2}{2} &= e_0 + \frac{p_0}{\rho_0} + \frac{D^2}{2} + q\end{aligned}\quad (6)$$

The subscripts 0 and 1 represent fresh and burned gases, respectively. The *sonic* condition, $(D - u_1)/c_1 = 1$, determines the CJ state.

a. *Approximate relations* Taking the limits $p_1/p_0 \gg 1$, and $e_1/e_0 \gg 1$, the wave Mach number and pressure are given by:

$$M_{CJ} \approx \left(\frac{2\rho_0(\gamma^2 - 1)q}{\gamma p_0(1 - b\rho_0)} \right)^{1/2}; \quad p_1 \approx \frac{2\rho_0(\gamma - 1)q}{(1 - b\rho_0)} \quad (7)$$

b. *Exact relations* Using the reduced variable, $q' = 2\rho_0 q/p_0(1 - b\rho_0)$, and after some algebra, the wave Mach number, pressure ratio and temperature ratio read:

“EOS influence on gaseous detonations”

$$M_{\text{CJ}} = \frac{1}{2} \left[\left(\frac{\gamma^2 - 1}{\gamma} q' \right)^{1/2} + \left(\frac{\gamma^2 - 1}{\gamma} q' + 4 \right)^{1/2} \right];$$

$$\frac{p_1}{p_0} = \frac{1 + \gamma M_{\text{CJ}}^2}{\gamma + 1}; \quad \frac{T_1}{T_0} = \left(\frac{1 + \gamma M_{\text{CJ}}^2}{(\gamma + 1) M_{\text{CJ}}} \right)^2 \quad (8)$$

2. von Neumann state

a. Approximate relations Taking the strong shock limit, $M_0 \gg 1$, and $q = 0$ in Eq. 6, the pressure, density and temperature ratios yield:

$$\frac{p_{\text{vN}}}{p_0} \approx \frac{2\gamma M_0^2}{\gamma + 1}; \quad \frac{\rho_0}{\rho_{\text{vN}}} \approx \frac{\gamma - 1}{\gamma + 1} + \frac{2b\rho_0}{\gamma + 1};$$

$$\frac{T_{\text{vN}}}{T_0} \approx \frac{2\gamma M_0^2(\gamma - 1)}{(\gamma + 1)^2} \quad (9)$$

b. Exact relations Rather tedious algebra¹ leads to the following expressions for the state variables ratios:

$$\frac{p_{\text{vN}}}{p_0} = \frac{2\gamma M_0^2 - (\gamma - 1)}{\gamma + 1};$$

$$\frac{\rho_0}{\rho_{\text{vN}}} = \frac{\gamma - 1}{\gamma + 1} + \frac{2 + 2b\rho_0(M_0^2 - 1)}{M_0^2(\gamma + 1)};$$

$$\frac{T_{\text{vN}}}{T_0} = 1 + \frac{2(M_0^2 - 1)(\gamma M_0^2 + 1)(\gamma - 1)}{M_0^2(\gamma + 1)^2} \quad (10)$$

The corrections due to NA in the CJ and vN states due to the co-volume b are explicitly shown.

III. COMPUTATIONAL METHODOLOGY

A. Numerical methods

The governing equations were integrated using our parallel in-house code RESIDENT (REcycling mesh SIMulations of DEtoNaTions)^{34–36}. Details about the numerical methods used for spatial and temporal discretizations as well as the parallelization methodology can

“EOS influence on gaseous detonations”

be found in Reynaud et al.³⁵. For completeness we provide a brief description here. Finite differences coupled with directional splitting are used for spatial discretization. An operator splitting method is performed to couple the hydrodynamics and the chemistry. The characteristic variables are reconstructed at the cell boundaries using a ninth order monotonicity preserving scheme³⁷. The fluxes at the interface are computed using the approximate Riemann solver of Toro (HLLC)³⁸, and a fix for the shear wave is also used to avoid the Carbuncle phenomenon³⁹. A third-order TVD explicit Runge-Kutta is used for the time integration with a CFL number of 0.2. This solver has been used successfully for fundamental studies using both simplified and detailed chemical kinetics³⁴.

B. Domain, initial and boundary conditions

A two-dimensional channel filled with reactive mixture, $Y_f = 1$, at $p_0 = 5$ MPa and $T_0 = 300$ K is considered. The channel dimensions are $L_x \times L_y = 300 l_{1/2} \times 150 l_{1/2}$, where $l_{1/2}$ corresponds to the ZND half reaction length (i.e. location where half of the reactant is consumed). The top and bottom boundaries are walls, whereas the left boundary is an outflow. The detonation is initiated by setting a circular area of $r_{\text{ign}} = 7 l_{1/2}$ at the vN state in the center of the channel. From this initiation procedure cylindrical shock waves are generated that reflect off the upper and lower boundaries, and subsequently focus resulting in a steady self-sustained detonation a few microseconds after.

A resolution of $\Delta x = \Delta y = l_{1/2}/20$ was used, and deemed sufficient based on a cell size grid independence study performed. Simulations were run in the laboratory frame of reference using a sliding window technique⁴⁰. During the simulation, as the detonation reaches the right boundary of the computational domain, a new region is added taken between the sonic plane and the left boundary. This is done to avoid disturbances emanating from the rear to penetrate the reaction zone and affect the detonation dynamics⁴¹. This method allows to have a fixed number of cells in the computational domain regardless of the length of the channel computed. Finally, the reaction was artificially inhibited when $Y_f < 10^{-3}$ to ensure that the reaction length remains finite. The total cost of the simulations is estimated at 0.5 million CPU hours for 18 million grid points per case, except for the marginal channel.

“EOS influence on gaseous detonations”

C. Mixture properties and kinetic parameters

The mixture is defined by γ , and its reactivity determined by the normalized activation energy E_a/RT_0 , and total energy content, q/RT_0 , whose values were set to 1.2, 20 and 50, respectively. The molecular weight of the mixture was $W = 12$ g/mol. The pre-exponential factors, A_s , were 1.10×10^9 s⁻¹ for PG, and 1.25×10^9 s⁻¹ for NA. The slightly higher value of A_s chosen for NA was so that the detonation half reaction length, $l_{1/2}$, was the same for both EOS used. We note that the set of parameters chosen lie below the 1-D stability boundary curve⁴² which permits to focus our analysis on instabilities coming only from the differences in EOS.

IV. RESULTS AND DISCUSSION

A. Steady traveling wave solution - ZND

Neglecting the time dependence in the governing equations and keeping one spatial dimension, the problem is reduced to a system of ordinary differential equations. Fixing the frame of reference to the detonation front ($x = 0$), the structure of the wave can be found by solving a boundary value problem. The solution procedure entails iterating on the inlet velocity imposed on the right boundary, D , while ensuring that on the left boundary the so-called sonic condition is satisfied.

Profiles for all state variables (p, ρ, T), as well as for the Mach number, M , are presented in Fig. 1 for both EOS. A few things are worth mentioning: (i) the pre-exponential values, A_s , for PG and NA were chosen such that the same half reaction length, $l_{1/2} = 6.71$ μm , was obtained; (ii) the co-volume, $b = 9.38 \times 10^{-4}$ m³/kg, for NA was selected to match the experimentally measured detonation velocity for a stoichiometric H₂-O₂ at $p_0 = 5$ MPa and $T_0 = 300$ K ($D_{\text{NA}} = 3150$ m/s)⁸; PG underpredicts the velocity by 2.25 % yielding a value of 3079 m/s; (iii) p_{vN} and T_{vN} are the same for both EOS whereas ρ_{vN} is ~ 17 % higher for PG. (iv) the rate at which the products are expanded is essentially the same with a slightly higher rate observed for NA (see p, ρ profiles) in Fig. 1. These results confirm the observations made in Section II B: ρ_{vN} is the only state variable in which the term $b\rho_0$ is present. Table I summarizes the input parameters used, as well as of CJ and vN states obtained for both EOS.

“EOS influence on gaseous detonations”

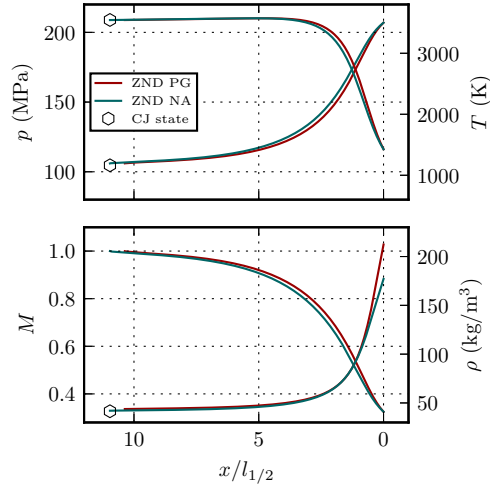


Figure 1: ZND profiles for PG and NA EOS. Co-volume, $b = 9.38 \times 10^{-4} \text{ m}^3$ chosen to match the experimentally measured detonation velocity for stoichiometric $\text{H}_2\text{-O}_2$. Conditions: $p_0 = 5 \text{ MPa}$; $T_0 = 300 \text{ K}$. Theoretical predictions of the CJ state for NA are shown as empty markers for reference: $p_{\text{CJ}} = 106.03 \text{ MPa}$, $T_{\text{CJ}} = 3546 \text{ K}$, $\rho_{\text{CJ}} = 41.48 \text{ kg/m}^3$.

B. Multidimensional unsteady results

In this section, we will compare the detonation front dynamics, the Favre-average profiles and the cellular structures obtained for both EOS.

1. Detonation front dynamics

In Fig. 2, instantaneous fields of Y_f with superimposed unity Mach number contours (measured in the frame of reference of the wave), normalized density gradients, $|\nabla\rho|/|\nabla\rho|_{\text{max}}$, and normalized vorticity $\omega/|\omega|_{\text{max}}$ are presented. The flow fields shown are a reduced portion of the computed domain focusing in the vicinity of the front. The overall detonation characteristics are well recovered and are qualitatively similar for both EOS. The detonation front structure can be readily observed in the $|\nabla\rho|/|\nabla\rho|_{\text{max}}$ fields where Mach stems and incident shocks are separated by triple points. Transverse waves travel along the leading

This is the author's peer reviewed, accepted manuscript. However, the online version of record will be different from this version once it has been copyedited and typeset.

PLEASE CITE THIS ARTICLE AS DOI: 10.1063/1.50040723

“EOS influence on gaseous detonations”

Table I: Summary of ZND results for both EOS.

	NA	PG
Initial conditions and mixture parameters		
p_0, T_0	5 MPa, 300 K	
γ	1.2	
E_a/RT_0	20	
q/RT_0	50	
b [m ³ /kg]	9.38×10^{-4}	—
A_s [s ⁻¹]	1.25×10^9	1.10×10^9
D [m/s]	3150	3079
$l_{1/2}$ [μm]	6.71	
vN State		
ρ_{vN}/ρ_0	7.43	8.70
p_{vN}/p_0	41	
T_{vN}/T_0	4.7	
CJ State		
ρ_{CJ}/ρ_0	1.76	1.79
p_{CJ}/p_0	21.5	
T_{CJ}/T_0	11.8	

shock interacting with shear layers. PG shows more transverse waves and triples points than NA, and an apparently shorter hydrodynamic thickness (i.e. distance from the leading shock to the sonic plane); see Y_f field. In Section IV B 2, this will be shown to be an artifact of visualizing a single instance, as the sonic plane has been documented to oscillate^{35,43}, and averaging is required to make any meaningful remark regarding its actual location. Finally, the vorticity fields show significantly more activity for PG than for NA. The increased strength and number of vortices present for PG will be directly linked with more *irregular* cellular structures in Section IV B 3.

Figure 3 (top) shows instantaneous velocity profiles obtained by tracking the position of the front in time at the bottom wall and taking a spatial probe. In Fig. 3 (bottom)

This is the author's peer reviewed, accepted manuscript. However, the online version of record will be different from this version once it has been copyedited and typeset.

PLEASE CITE THIS ARTICLE AS DOI: 10.1063/1.50040723

“EOS influence on gaseous detonations”

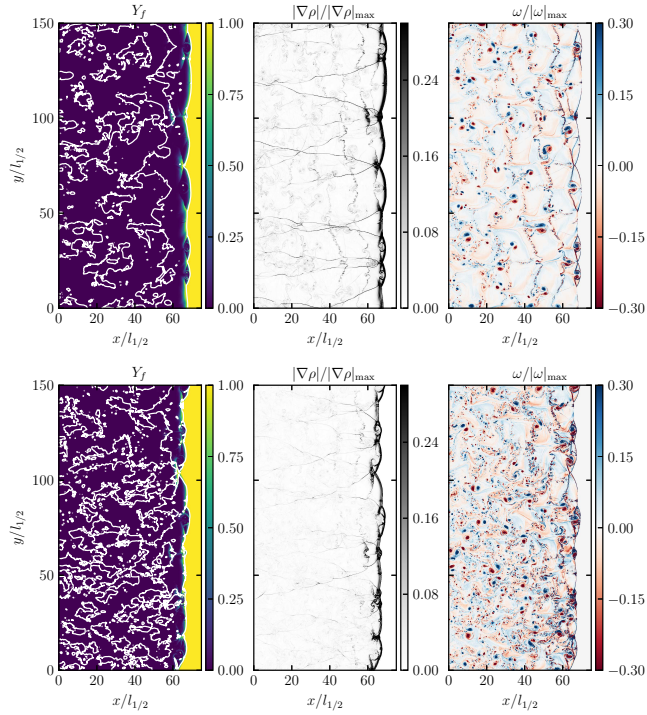


Figure 2: Instantaneous fuel mass fraction, Y_f , with superimposed unity Mach number contours (solid white lines), normalized density gradient, $|\nabla\rho|/|\nabla\rho|_{max}$, and normalized vorticity, $\omega/|\omega|_{max}$, for NA (top) and PG (bottom). Conditions: $p_0 = 5$ MPa, $T_0 = 300$ K.

the probability density function (pdf) of the leading shock velocity is shown. Distances and velocities are normalized by $l_{1/2}$ and D_{CJ} , respectively. The overall behavior is very similar for both EOS, their range of oscillations are $0.7 < D/D_{CJ} < 1.6$ for PG, and $0.8 < D/D_{CJ} < 1.8$ for NA; only slight differences are present at their extrema values. Detonations naturally adopt an unstable and oscillatory behaviour, which affects locally the detonation velocity. The peaks come from triple points collisions, whereas the troughs are the result of local expansions across the front due to curvature and the presence of reactivity gradients. The process repeats itself upon new triple points collisions. The pdf follows the same trend for both EOS, with the most likely front velocity lying around $D/D_{CJ} \sim 0.9$. The power-law dependence alluded to in previous work⁴⁴ seems to breakdown exhibiting a

“EOS influence on gaseous detonations”

flat region for $1.05 < D/D_{CJ} < 1.3$.

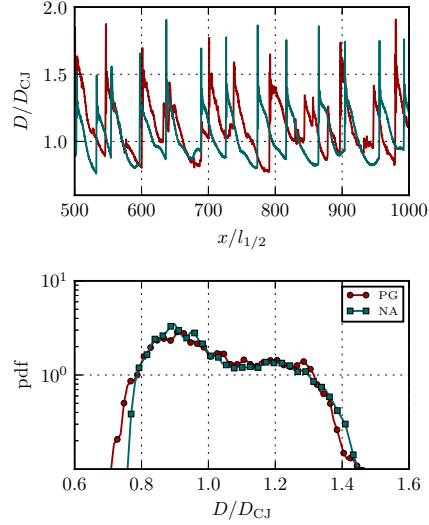


Figure 3: 2-D detonation front dynamics (top) and probability density function of the normalized detonation velocity, D/D_{CJ} (bottom) for PG and NA. Conditions: $p_0 = 5$ MPa, $T_0 = 300$ K.

2. Favre averages and comparison with ZND

Two-dimensional (2-D) Favre averages were obtained by taking all the profiles along the height of the channel, L_y , making them collapse into one line after changing the frame of reference to be fixed to the wave (i.e. $(x - x_s(y, t))$; $x_s(y, t)$ is the instantaneous leading shock location), and subsequently performing a temporal averaging as per the following expression^{35,43,45,46}:

$$\bar{G} = \frac{1}{L_y} \int_0^{L_y} \left\{ \lim_{T \rightarrow \infty} \left(\frac{1}{T} \int^T G(x - x_s(y, t), y, t) dt \right) \right\} dy \quad (11)$$

A clear comparison of the mean structures can thus be obtained for NA and PG; note that three grid points at the top and bottom boundaries are excluded while evaluating the integral to avoid numerical artifacts. Figure 4 shows profiles of p , T , ρ , and M where

This is the author's peer reviewed, accepted manuscript. However, the online version of record will be different from this version once it has been copyedited and typeset.

PLEASE CITE THIS ARTICLE AS DOI: 10.1063/1.50040723

“EOS influence on gaseous detonations”

the averaged thermodynamic quantities are compared with the laminar ZND structure. The main differences observed between the ZND and Favre averages are due to 2-D hydrodynamic fluctuations that have been shown to delay the mean sonic location^{35,43,47}, even if the value of E_a/RT_0 selected is rather low. For the case studied, the Favre averages do not show significant differences between the EOS.

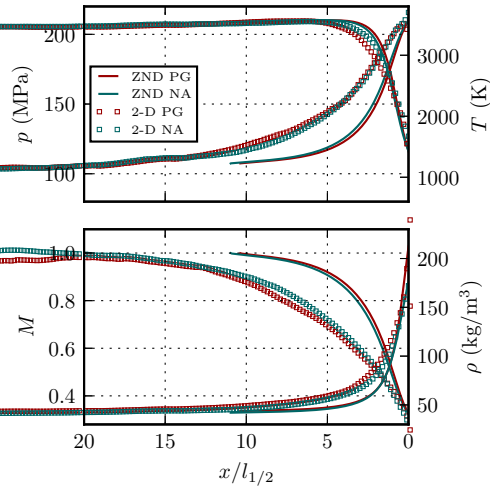


Figure 4: Comparison of Favre averages from 2-D unsteady computation with ZND profiles obtained using PG and NA EOS. $p_0 = 5$ MPa, $T_0 = 300$ K.

3. Soot foils

Figure 5 shows a comparison of a portion of the soot foils obtained after running the simulations using PG and NA. Distances are normalized by $l_{1/2}$. Histograms showing the distribution of cell sizes are also included in this figure. These were obtained by manually measuring all the length scales present (75 samples per case), and subsequently sorting the data by number of occurrences of a given scale, i.e. Frequency (#). The detonation cell sizes are in the range of $9 l_{1/2} < \lambda_{PG} < 37 l_{1/2}$ for PG, and $7 l_{1/2} < \lambda_{NA} < 35 l_{1/2}$ for NA. While the average cell size is essentially the same for both EOS ($\sim 20 l_{1/2}$), the soot foil for PG exhibits more *irregular* structures than those present in the soot foil obtained for

“EOS influence on gaseous detonations”

NA. The histograms provide quantitative evidence for the latter statement, PG has a broad distribution with a high number of occurrences at different length scales, whereas NA shows higher frequencies in a narrower range of length scales with its maximum centered around $25 l_{1/2}$, i.e., a sign of a more *regular* structure. This outcome indicates that something fundamentally different is taking place at the detonation front.

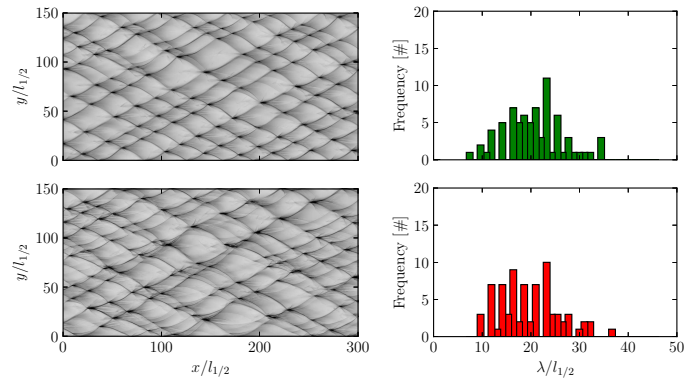


Figure 5: Numerical soot foils and cell size distributions obtained using NA (top) and PG (bottom) EOS. $p_0 = 5$ MPa, $T_0 = 300$ K.

Figure 6 shows a closeup to the soot foils for both EOS. Notably for PG, there is generation of new triple points, not over one cell, but as a longer process that takes 4-5 cells to develop (see arrows in Fig. 6). The disturbances generated upon a triple point collision initially (1.), fade away (2.), and subsequently get amplified (3-5.) upon interaction with other triple points to become finally a new triple point (5.).

The amplification process that results in the formation of a new triple point appears to have been identified. However, the origin of these disturbances remain to be determined. This will be discussed in the following section.

4. Source of perceived instabilities

The different cellular structure obtained for PG and NA, even though γ , E_a/RT_0 and q/RT_0 for both cases were kept fixed, warrants a deeper investigation into the source of the perceived instabilities. To examine this process, additional simulations were run for both

“EOS influence on gaseous detonations”

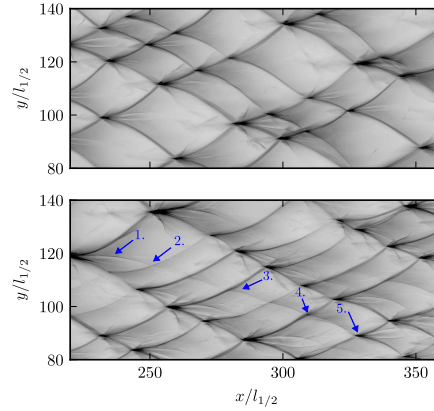


Figure 6: Close-up to numerical soot foils, $x/l_{1/2} \in [220, 360]$, $y/l_{1/2} \in [80, 140]$, obtained using NA (top) and PG (bottom) EOS. Conditions: $p_0 = 5$ MPa, $T_0 = 300$ K.

EOS using a reduced channel height ($L_y = 0.8 \lambda$). A time sequence showing fields of the normalized temperature, T/T_0 , density gradient, $|\nabla\rho|/|\nabla\rho|_{\max}$, and pressure, $|\nabla p|/|\nabla p|_{\max}$, are included in Fig. 7 for NA (top) and PG (bottom).

The sequence for NA presents the classical behaviour of marginal detonations. The $|\nabla\rho|/|\nabla\rho|_{\max}$ fields allow to identify the incident shock (i) and Mach stem (m). At $t_{\text{NA}} = 101.53 \mu\text{s}$, a transverse shock wave (t) reflected from the upper boundary propagates downward. A Mach stem (m) is then formed in the upper part of the detonation front attached to the triple point (a) located at $(x/l_{1/2}, y/l_{1/2}) = (10.5, 7)$. An additional transverse shock connects the triple point (b) to (a) to form a Double irregular Mach Reflection (DiMR)⁴⁸. The Mach stem is characterized by a thinner induction zone than that behind the incident shock as seen in the temperature fields. A slip line (s) separates the gas burned by the Mach stem from the gas processed by the incident shock; it starts from the triple point (a), rolling towards the upper boundary. From the phenomenology of irregular Mach reflections for strong shocks, the stagnation pressure behind the stem is high enough to induce jetting into the flow. This jet is typically oriented towards the detonation propagation direction^{49,50} and would most probably be amplified with increasing heat release.

A second slip line (r) is visible downstream of the front at $(x/l_{1/2}, y/l_{1/2}) = (5, 10)$ separating a reactive unburnt pocket from the surrounding burned gas. The line (b-c) forms

“EOS influence on gaseous detonations”

a shock that interacts with the slip line (s) (see $|\nabla p|/|\nabla p|_{\max}$ fields). At $t_{\text{NA}} = 101.55 \mu\text{s}$, the triple point (a) moves downwards. The Mach stem weakens as can be seen from the increasing distance between the leading shock and reaction zone. A transverse wave impacts the bottom boundary at $(x/l_{1/2}, y/l_{1/2}) = (0, 0)$, interacting with a vortex formed by a jet in a previous cycle. At $t_{\text{NA}} = 101.56 \mu\text{s}$, the triple point reaches the bottom boundary; the reflected transverse waves now propagate upwards. The triple points (b) and (c), and the slip line (s) are detached from the front and convected downstream $(x/l_{1/2}, y/l_{1/2}) = (7, 0)$, as well as the vortical structure at the upper boundary. The detonation starts a new cycle. Note that at $t_{\text{NA}} = 101.59 \mu\text{s}$ the flow is symmetric with respect to $y/l_{1/2, \max}$ at $t_{\text{NA}} = 101.53 \mu\text{s}$.

The previous flow description is also applicable to the PG Fields. However, the forward jet formed at the upper boundary at $t_{\text{PG}} = 109.12 \mu\text{s}$ impinges on the Mach stem inducing a front distortion illustrated by a discontinuous change in curvature. The latter is the origin of the formation of point k_2 that interacts with the upper boundary and reflects afterwards. The shock waves attached to this triple point (a) get weaker until becoming pressure waves at $t_{\text{PG}} = 109.21 \mu\text{s}$ (see weak gradients (pw) in the $|\nabla p|/|\nabla p|_{\max}$ fields) leaving only a slip line in the $|\nabla \rho|/|\nabla \rho|_{\max}$ fields. Similarly, point k_1 is formed through the same mechanism from previous interactions, and collides with the triple point (a) as seen in $t_{\text{PG}} = 109.15\text{--}109.16 \mu\text{s}$. Upon this interaction, k_1 becomes a triple point at $t_{\text{PG}} = 109.16 \mu\text{s}$, and continues its propagation toward the upper boundary ($t_{\text{PG}} = 109.21 \mu\text{s}$). Finally, at $t_{\text{PG}} = 109.21 \mu\text{s}$, the slip line connected to point k_1 perturbs the transverse wave (t) attached to the triple point (a). These results suggest that the jet interaction with the Mach stem that arises from the triple point reflection at the boundary is the triggering mechanism of front distortion/bifurcation and subsequent formation of new triple points.

Mach stem bifurcations under jetting, similar to those described above, were reported by Sharpe⁵¹. The jet impact on the leading shock results in the formation of vortices, however, it is difficult from simulations alone to determine whether the shock-vortex interaction is responsible for the genesis of the triple points, or whether it is just an aiding mechanism. Clavin⁵² provided supporting evidence through a linear analysis using the strong shock approximation at the Newtonian limit, i.e., $(\gamma - 1) \rightarrow 0$. According to his analysis, the interaction of a shock wave with a vortex can indeed enhance Mach stem and triple point formation. It was postulated that all these additional triple points could potentially result in more irregular cellular structures. Shock bifurcations were also numerically shown to occur

This is the author's peer reviewed, accepted manuscript. However, the online version of record will be different from this version once it has been copyedited and typeset.

PLEASE CITE THIS ARTICLE AS DOI: 10.1063/1.50040723

“EOS influence on gaseous detonations”

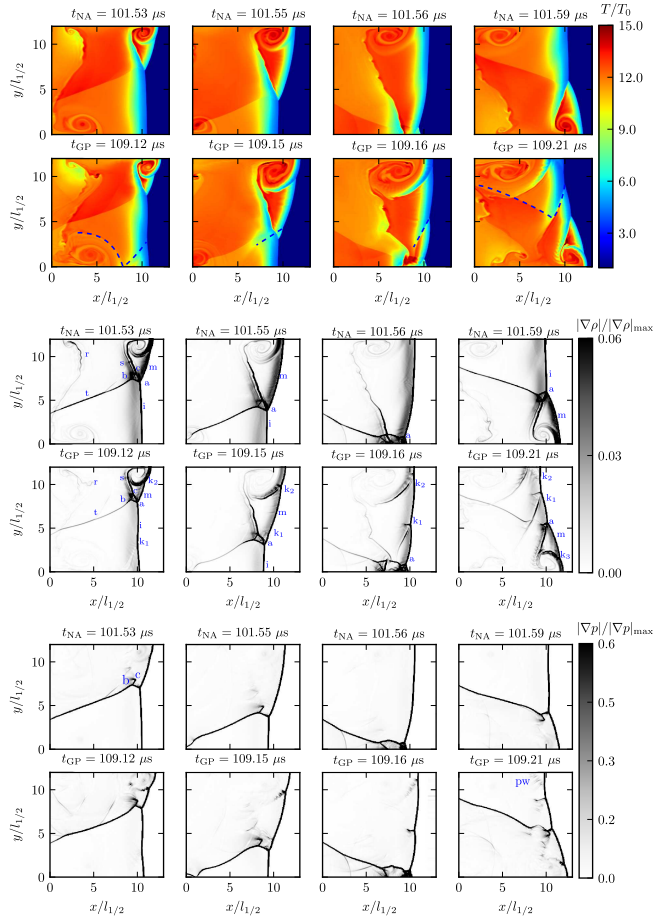


Figure 7: Normalized temperature T/T_0 , normalized density gradient $|\nabla\rho|/|\nabla\rho|_{\max}$ and pressure $|\nabla p|/|\nabla p|_{\max}$ obtained using NA (top) and PG (bottom) EOS for a marginal channel ($L_y = 0.8 \lambda$). Conditions: $p_0 = 5$ MPa, $T_0 = 300$ K.

with inert triple points through the examination of shock reflections over a ramp⁵³. The authors found that for $\gamma = 1.2$, a ramp angle of 20° , and a shock strength of $M \sim 6$ the Mach stem bifurcates. This angle, however, is lower than the usual triple point reflection angle observed in detonations ($\sim 34^\circ$)⁵⁴. Mach and Radulescu⁵⁵ proposed a cell multiplication mechanism whereby there is creation of wave bifurcations on the detonation front following

“EOS influence on gaseous detonations”

Table II: Propensity to develop inert shock bifurcations. Adapted from Mach & Radulescu⁵⁵ and Lau-Chapdelaine⁵⁶.

γ	Bifurcation	Cellular structure
≤ 1.3	Yes	Irregular
1.2/1.3	Yes	Intermediate
≥ 1.41	No	Regular

triple point collisions. These new triple points, upon interaction with already existing triple points, can give rise to additional cells. Their description bears close resemblance with our observations above. The authors supported their arguments using existing experimental data in which the conditions conducive to shock bifurcations on the leading shock of gaseous detonations were compared against mixtures for which observations of cellular *irregularity* is available. Over 20 data points (mixtures) were collected and summarized in the form of a table in their paper, specifying the initial pressure, leading shock Mach number, M_{CJ} , ratio of specific heats, γ , type of cellular structure, and whether inert shock reflections at the specified conditions (γ and M_{CJ}) resulted in shock bifurcations. Here, for completeness, we include a shortened version of this table only specifying, as a function of γ , the type of cellular structure observed and the presence of shock bifurcations.

Table II shows a clear trend. For $\gamma \leq 1.3$, inert shock reflections for the respective M_{CJ} of the mixtures analyzed result in bifurcations and *irregular* cellular structures. For $\gamma \geq 1.41$ the opposite holds. The cellular structure for $\gamma = 1.32$ and 1.2 were deemed as *intermediate*. Based on these observations it seems that the cellular structure of gaseous detonations can be directly linked to their propensity to develop inert shock bifurcations which in turn seems to be very sensitive to γ . Put differently, an incremental change in γ of 0.1 changes the cellular structure of gaseous detonations from *irregular* to *regular*. Note, however, that all the data collected and analysis done considered atmospheric and sub-atmospheric initial pressures^{55,56}. Yet, their work indicates that the extent of visible bifurcations that occur at the leading shock, resulting in the formation of new triple points, seems to be a function of γ . More specifically, these bifurcations become more frequent as γ approaches unity; Chapdelaine et al.⁵⁷ and Sow et al.⁵⁸ reported similar observations while studying inert shock reflections and detonation propagation in marginal channels at

“EOS influence on gaseous detonations”

low initial pressures.

We can compute the isentropic coefficient, $\chi_s = (\rho/p) \cdot (\partial p / \partial \rho)_s$, for both EOS to assess if there are effective changes that may be responsible for the more irregular structure obtained for NA. The relevant state to investigate any structure developing at the detonation front, and in particular, those associated with inert shock instabilities is the vN state. The expressions for χ_s are:

$$\chi_{s,PG} = \gamma; \quad \chi_{s,NA} = \frac{\gamma}{(1 - b\rho_{vN})} \quad (12)$$

For PG, $\chi_{s,PG}$ is equal to the ratio of specific heats $\chi_{s,PG} = \gamma = 1.2$. For NA, the co-volume and density at the vN state enter the expression for χ_s . Using the post-shock value obtained from the 2-D Favre Averages, which provides a more representative metric of the temporal evolution of the vN state, results in $\chi_{s,NA} \simeq 1.42$. The increase in χ_s obtained suggests that the change in the nature of the detonation wave may come from having a mixture whose propensity to develop inert shock instabilities is less, crossing over the two γ boundaries listed in table II. This result appears to explain the change in multi-cellular structure between the EOS.

To confirm these observations, additional numerical simulations were run. Since $\chi_{s,NA}$ is an increasing function of $b\rho_{vN}$, using a higher co-volume value increases $\chi_{s,NA}$ and, provided that our hypothesis is valid, it should yield a more regular cellular structure. Two different initial pressures $p_0 = 7.5$ MPa and $p_0 = 10$ MPa were considered. The corresponding co-volumes $b_{7.5\text{MPa}} = 1.305 \times 10^{-3} \text{ m}^3/\text{kg}$ and $b_{10\text{MPa}} = 1.45 \times 10^{-3} \text{ m}^3/\text{kg}$ were found using the same methodology described above. Namely, by varying b and A_s to match the steady detonation velocities ($D_{CJ,7.5\text{MPa}} = 3220$ m/s and $D_{CJ,10\text{MPa}} = 3297$ m/s) and half-reaction lengths ($l_{1/2,7.5\text{MPa}} = 2.5 \mu\text{m}$ and $l_{1/2,10\text{MPa}} = 2.0 \mu\text{m}$) reported in Schmidt and Butler⁵⁹ at the selected pressures; the pre-exponentials are $A_{s,7.5\text{MPa}} = 3.75 \times 10^9 \text{ s}^{-1}$ and $A_{s,10\text{MPa}} = 5.25 \times 10^9 \text{ s}^{-1}$ for NA, and $A_{s,7.5\text{MPa}} = 2.98 \times 10^9 \text{ s}^{-1}$ and $A_{s,10\text{MPa}} = 3.70 \times 10^9 \text{ s}^{-1}$ for PG. The ZND profiles for the different initial conditions are presented in Fig. 8. Note the increase in p_{vN} with increasing initial pressure despite a constant T_{vN} .

The soot foils are presented in Fig. 9, note that an additional soot foil at atmospheric pressure is also included for reference. While the cellular structure obtained for PG remains *irregular* and largely unaffected by the initial pressure, for NA, changes in the cellular structure as a function of p_0 are evident. Further quantitative evidence is provided by the

This is the author's peer reviewed, accepted manuscript. However, the online version of record will be different from this version once it has been copyedited and typeset.

PLEASE CITE THIS ARTICLE AS DOI: 10.1063/1.50040723

“EOS influence on gaseous detonations”

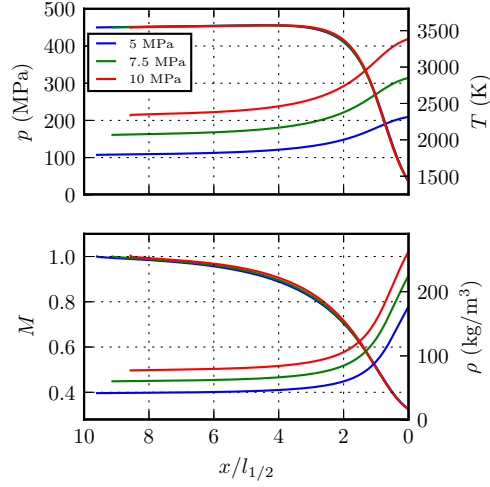


Figure 8: ZND profiles obtained for NA using three different initial pressures $p_0 = 5.0$ MPa, $p_0 = 7.5$ MPa and $p_0 = 10.0$ MPa. Distance is normalized by their respective half-reaction lengths: $l_{1/2,5\text{ MPa}} = 6.7$ μm , $l_{1/2,7.5\text{ MPa}} = 2.5$ μm and $l_{1/2,10\text{ MPa}} = 2.0$ μm .

narrowing histograms showing the convergence towards a reduced range of length scales. In line with the arguments presented above a higher value of χ_s ($\chi_{s,NA,7.5\text{ MPa}} = 1.70$ and $\chi_{s,NA,10\text{ MPa}} = 1.94$) yields more *regular* cellular structures. It is worth emphasizing that the post-shock temperature, T_{vN} , is constant in the cases considered, hence the *irregularity* obtained does not come from changes in the reduced activation energy, $E_a/R_u T_{vN}$ (see Fig. 8). Finally, the average cell size decreases with $l_{1/2}$ but the ratio $\lambda/l_{1/2}$ is almost constant in the range of pressures tested with values of 18.2, 19.59 and 20.38 for $p_0 = 5.0$, 7.5 and 10 MPa, respectively. For completeness, results for the same pressures range but keeping the pre-exponential factor, A_s , fixed for both EOS are shown in the Appendix. The fundamental change in the nature of the wave is thus an outcome that can be unequivocally attributed to the different EOS used.

This is the author's peer reviewed, accepted manuscript. However, the online version of record will be different from this version once it has been copyedited and typeset.

PLEASE CITE THIS ARTICLE AS DOI: 10.1063/5.0040723

“EOS influence on gaseous detonations”

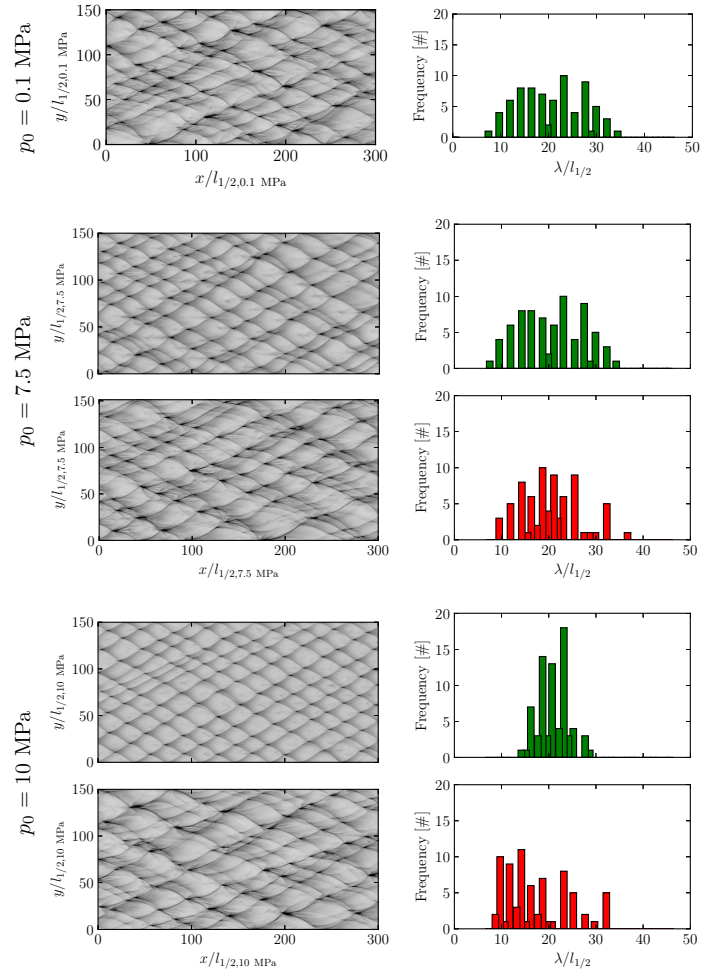


Figure 9: Numerical soot foils obtained using NA (top) and PG (bottom) for $p_0 = 7.5$ MPa and 10 MPa whose effective χ_s values are 1.7 and 1.94. A sootfoil for $p_0 = 0.1$ MPa is shown for reference where the NA and PG descriptions are equivalent ($\chi_s = 1.2$). Results for $p_0 = 5$ MPa are included in Fig. 5.

“EOS influence on gaseous detonations”

V. CONCLUSION

Two-dimensional numerical simulations of gaseous detonations at initial elevated pressures were performed. Two EOS, PG and NA, were compared to determine whether real gas effects influence the cellular structure of gaseous detonations. Results show that neglecting these effects renders a more *irregular* structure. The mechanism of cell multiplication was investigated and consists of two phases: an initial jet-Mach stem interaction that results in a perturbed leading shock, followed by gradual growth of this perturbation over a few cells, caused by a shear-layer triple point interaction. Analysis of our results in terms of the isentropic coefficient χ_s , and comparison with previous experimental and numerical data showed that the more *regular* structure obtained for NA may come from effectively having a mixture whose propensity to develop inert shock instabilities is less. Further investigation of the cell multiplication mechanism identified as a function of heat release, as well as the exploration of pressure dependent reaction rates, dynamic co-volumes, i.e., $b = f(\rho)$ and alternative analytical forms to describe deviations from perfect gas behavior will be a topic of future work.

ACKNOWLEDGEMENTS

The authors thank H. El-Rabii for valuable discussions on this work. The computations were performed using HPC resources from the cluster of Pprime, the Mésocentre de Calcul Poitevin and from GENCI-CINES (Grant 2018-A0052B07735). This work was supported by the CPER FEDER Project of Région Nouvelle Aquitaine.

DATA AVAILABILITY

The data that support the findings of this study are available from the corresponding author upon reasonable request.

This is the author's peer reviewed, accepted manuscript. However, the online version of record will be different from this version once it has been copyedited and typeset.

PLEASE CITE THIS ARTICLE AS DOI: 10.1063/1.50040723

“EOS influence on gaseous detonations”

REFERENCES

- ¹W. Fickett and W. C. Davis, *Detonation: theory and experiment* (Courier Corporation, 2000).
- ²S. Hansmetzger, R. Zitoun, and P. Vidal, “A study of continuous rotation modes of detonation in an annular chamber with constant or increasing section,” *Shock Waves* **28**, 1065–1078 (2018).
- ³J. Z. Ma, M.-Y. Luan, Z.-J. Xia, J.-P. Wang, S.-j. Zhang, S.-b. Yao, and B. Wang, “Recent progress, development trends, and consideration of continuous detonation engines,” *AIAA Journal* **58**, 4976–5035 (2020).
- ⁴D. Lim, J. Humble, and S. D. Heister, “Experimental testing of an rp-2-gox rotating detonation rocket engine,” in *AIAA Scitech 2020 Forum* (2020) p. 0195.
- ⁵J. Humble and S. D. Heister, “Heterogeneous detonation physics as applied to high pressure rotating detonation engines,” in *AIAA Scitech 2021 Forum* (2021) p. 1027.
- ⁶F. Bykovskii, S. Zhdan, E. Vedernikov, A. Samsonov, and E. Popov, “Continuous detonation of a mixture of gaseous hydrogen and liquid oxygen in a plane–radial combustor with exhaustion toward the periphery,” *Combustion, Explosion, and Shock Waves* **56**, 682–690 (2020).
- ⁷G. Chamberlain, E. Oran, and A. Pekalski, “Detonations in industrial vapour cloud explosions,” *Journal of Loss Prevention in the Process Industries* **62**, 103918 (2019).
- ⁸R. Schmitt and P. Butler, “Detonation properties of gases at elevated initial pressures,” *Combustion Science and Technology* **106**, 167–191 (1995).
- ⁹H. W. Liepmann and A. Roshko, *Elements of gasdynamics* (Courier Corporation, 2001).
- ¹⁰R. L. Gealer and S. W. Churchill, “Detonation characteristics of hydrogen-oxygen mixtures at high initial pressures,” *AIChE Journal* **6**, 501–505 (1960).
- ¹¹R. E. Duff, “Investigation of spinning detonation and detonation stability,” *The physics of fluids* **4**, 1427–1433 (1961).
- ¹²B. Levitt and D. Hornig, “Structure of detonation waves in gases,” *The Journal of Chemical Physics* **36**, 219–227 (1962).
- ¹³V. Manzhalei, V. Mitrofanov, and V. Subbotin, “Measurement of inhomogeneities of a detonation front in gas mixtures at elevated pressures,” *Combustion, Explosion and Shock Waves* **10**, 89–95 (1974).

This is the author's peer reviewed, accepted manuscript. However, the online version of record will be different from this version once it has been copyedited and typeset.

PLEASE CITE THIS ARTICLE AS DOI: 10.1063/1.50040723

- “EOS influence on gaseous detonations”
- ¹⁴P. Bauer, C. Brochet, and S. Krishnan, “Detonation characteristics of gaseous ethylene, oxygen, and nitrogen at high initial pressures,” *Gasdynamics of detonations and explosions*, 408–422 (1981).
- ¹⁵P. Bauer and C. Brochet, “The structure of the detonation front in explosive mixtures at high pressures,” *Arch. Comb.* **3**, 39–45 (1983).
- ¹⁶P. Bauer and C. Brochet, “Properties of detonation waves in hydrocarbon-oxygen-nitrogen mixtures at high initial pressures,” *Shock waves, explosions, and detonations*(A 84-28376 12-34). New York, American Institute of Aeronautics and Astronautics, Inc., 1983, , 231–243 (1983).
- ¹⁷P. Bauer, H. Presles, O. Heuze, and C. Brochet, “Measurement of cell lengths in the detonation front of hydrocarbon oxygen and nitrogen mixtures at elevated initial pressures,” *Combustion and Flame* **64**, 113–123 (1986).
- ¹⁸P. A. Bauer, M. Giraud, J.-F. Legendre, and L. Catoire, “Detonability limits of methane-oxygen mixtures at elevated initial pressures,” *Propellants, Explosives, Pyrotechnics* **19**, 311–314 (1994).
- ¹⁹N. Astapov, Y. A. Nikolaev, and V. Y. Ul’yanitskii, “Detonation parameters of hydrogen-oxygen and hydrogen-air mixtures at high initial density,” *Combustion, Explosion, and Shock Waves* **20**, 89–96 (1984).
- ²⁰O. Heuzé, “Equations of state of detonation products: Influence of the repulsive intermolecular potential,” *Physical Review A* **34**, 428 (1986).
- ²¹W. A. Sirignano, “Normal shocks with high upstream pressure,” *Physical Review Fluids* **3**, 093401 (2018).
- ²²W. A. Sirignano, “Compressible flow at high pressure with linear equation of state,” *Journal of Fluid Mechanics* **843**, 244–292 (2018).
- ²³R. Anand, “Jump relations across a shock in non-ideal gas flow,” *Astrophysics and Space Science* **342**, 377–388 (2012).
- ²⁴P. Tudisco and S. Menon, “Numerical investigations of phase-separation during multi-component mixing at super-critical conditions,” *Flow, Turbulence and Combustion* **104**, 693–724 (2020).
- ²⁵P. Tudisco and S. Menon, “A vapor–liquid equilibrium induced lewis number effect in real-gas shear layers: A theoretical study,” *Physics of Fluids* **32**, 112111 (2020).

This is the author's peer reviewed, accepted manuscript. However, the online version of record will be different from this version once it has been copyedited and typeset.

PLEASE CITE THIS ARTICLE AS DOI: 10.1063/1.50040723

- “EOS influence on gaseous detonations”
- ²⁶O. Le Métayer and R. Saurel, “The noble-abel stiffened-gas equation of state,” *Physics of Fluids* **28**, 046102 (2016).
- ²⁷M. Radulescu, “On the noble-abel stiffened-gas equation of state,” *Physics of Fluids* **31**, 111702 (2019).
- ²⁸M. I. Radulescu, “Compressible flow in a noble–abel stiffened gas fluid,” *Physics of Fluids* **32**, 056101 (2020).
- ²⁹P. Boivin, M. Cannac, and O. Le Metayer, “A thermodynamic closure for the simulation of multiphase reactive flows,” *International Journal of Thermal Sciences* **137**, 640–649 (2019).
- ³⁰A. Chiapolino and R. Saurel, “Extended noble-abel stiffened-gas equation of state for sub-and-supercritical liquid-gas systems far from the critical point,” *Fluids* **3**, 48 (2018).
- ³¹M. I. Radulescu, *The propagation and failure mechanism of gaseous detonations: experiments in porous-walled tubes*, Ph.D. thesis, McGill University (2003).
- ³²H. D. Ng, *The effect of chemical reaction kinetics on the structure of gaseous detonation*, Ph.D. thesis, McGill University (2005).
- ³³M. Short and J. Dold, “Linear stability of a detonation wave with a model three-step chain-branching reaction,” *Mathematical and Computer Modelling* **24**, 115–123 (1996).
- ³⁴S. Taileb, J. Melguizo-Gavilanes, and A. Chinnayya, “Influence of the chemical modeling on the quenching limits of gaseous detonation waves confined by an inert layer,” *Combustion and Flame* **218**, 247–259 (2020).
- ³⁵M. Reynaud, F. Viot, and A. Chinnayya, “A computational study of the interaction of gaseous detonations with a compressible layer,” *Physics of Fluids* **29**, 056101 (2017).
- ³⁶M. Reynaud, S. Taileb, and A. Chinnayya, “Computation of the mean hydrodynamic structure of gaseous detonations with losses,” *Shock Waves* **30**, 645–669 (2020).
- ³⁷A. Suresh and H. T. Huynh, “Accurate monotonicity-preserving schemes with runge–kutta time stepping,” *Journal of Computational Physics* **136**, 83–99 (1997).
- ³⁸E. F. Toro, M. Spruce, and W. Speares, “Restoration of the contact surface in the hll-riemann solver,” *Shock waves* **4**, 25–34 (1994).
- ³⁹Z. Shen, W. Yan, and G. Yuan, “A robust hllc-type riemann solver for strong shock,” *Journal of Computational Physics* **309**, 185–206 (2016).
- ⁴⁰A. Sow, A. Chinnayya, and A. Hadjadj, “On the viscous boundary layer of weakly unstable detonations in narrow channels,” *Computers & Fluids* **179**, 449–458 (2019).

This is the author's peer reviewed, accepted manuscript. However, the online version of record will be different from this version once it has been copyedited and typeset.

PLEASE CITE THIS ARTICLE AS DOI: 10.1063/1.50040723

“EOS influence on gaseous detonations”

- ⁴¹G. I. Taylor, “The dynamics of the combustion products behind plane and spherical detonation fronts in explosives,” *Proceedings of the Royal Society of London. Series A. Mathematical and Physical Sciences* **200**, 235–247 (1950).
- ⁴²H. D. Ng, M. I. Radulescu, A. J. Higgins, N. Nikiforakis, and J. H. Lee, “Numerical investigation of the instability for one-dimensional chapman–jouguet detonations with chain-branching kinetics,” *Combustion Theory and Modelling* **9**, 385–401 (2005).
- ⁴³A. Sow, A. Chinnayya, and A. Hadjadj, “Mean structure of one-dimensional unstable detonations with friction,” *Journal of Fluid Mechanics* **743**, 503–533 (2014).
- ⁴⁴B. M. Maxwell, R. R. Bhattacharjee, S. S. Lau-Chapdelaine, S. A. Falle, G. J. Sharpe, and M. I. Radulescu, “Influence of turbulent fluctuations on detonation propagation,” *Journal of Fluid Mechanics* **818**, 646–696 (2017).
- ⁴⁵H. Watanabe, A. Matsuo, A. Chinnayya, K. Matsuoka, A. Kawasaki, and J. Kasahara, “Numerical analysis of the mean structure of gaseous detonation with dilute water spray,” *Journal of Fluid Mechanics* **887** (2020).
- ⁴⁶S. Taieb, M. Reynaud, A. Chinnayya, F. Viot, and P. Bauer, “Numerical study of 3d gaseous detonations in a square channel,” *Aerotecnica Missili & Spazio* **97**, 96–102 (2018).
- ⁴⁷M. I. Radulescu, G. J. Sharpe, C. K. Law, and J. H. Lee, “The hydrodynamic structure of unstable cellular detonations,” *Journal of Fluid Mechanics* **580**, 31–81 (2007).
- ⁴⁸G. Ben-Dor, *Shock wave reflection phenomena*, Vol. 2 (Springer, 2007).
- ⁴⁹P. Mach, *Bifurcating Mach Shock Reflections with Application to Detonation Structure*, Master’s thesis, University of Ottawa (2011).
- ⁵⁰H. Hornung and M. Robinson, “Transition from regular to mach reflection of shock waves part 2. the steady-flow criterion,” *Journal of Fluid Mechanics* **123**, 155–164 (1982).
- ⁵¹G. J. Sharpe, “Transverse waves in numerical simulations of cellular detonations,” *Journal of Fluid Mechanics* **447**, 31–51 (2001).
- ⁵²P. Clavin, “Nonlinear analysis of shock–vortex interaction: Mach stem formation,” *Journal of Fluid Mechanics* **721**, 324–339 (2013).
- ⁵³M. I. Radulescu, A. Papi, J. J. Quirk, P. Mach, and B. M. Maxwell, “The origin of shock bifurcations in cellular detonations,” in *22nd International Colloquium on the Dynamics of Explosions and Reactive Systems* (2009) p. 4.
- ⁵⁴M. I. Radulescu, G. J. Sharpe, C. K. Law, and J. H. Lee, “The hydrodynamic structure of unstable cellular detonations,” *Journal of Fluid Mechanics* **580**, 31–81 (2007).

This is the author's peer reviewed, accepted manuscript. However, the online version of record will be different from this version once it has been copyedited and typeset.

PLEASE CITE THIS ARTICLE AS DOI: 10.1063/5.0040723

“EOS influence on gaseous detonations”

- ⁵⁵P. Mach and M. I. Radulescu, “Mach reflection bifurcations as a mechanism of cell multiplication in gaseous detonations,” *Proceedings of the Combustion Institute* **33**, 2279–2285 (2011).
- ⁵⁶S. S.-M. Lau-Chapdelaine, *Viscous triple shock reactions relevant to detonation waves, and Detonation dynamics predicted by the Fickett model*, Ph.D. thesis, University of Ottawa, Canada (2019).
- ⁵⁷S. S.-M. Lau-Chapdelaine, Q. Xiao, and M. I. Radulescu, “Viscous jetting and mach stem bifurcation in shock reflections: experiments and simulations,” *Journal of Fluid Mechanics* **908**, A18 (2021).
- ⁵⁸A. Sow, S. S. Lau-Chapdelaine, and M. Radulescu, “The effect of the polytropic index γ on the structure of gaseous detonations,” *Proceedings of the Combustion Institute* (2020).
- ⁵⁹R. Schmitt and P. Butler, “Detonation wave structure of gases at elevated initial pressures,” *Combustion science and technology* **107**, 355–385 (1995).

APPENDIX

Additional simulations were run to test whether the different pre-exponential factors used to keep the half-reaction lengths fixed influence the observed *regularization* of the cellular structure. Figure 10 shows the numerical soot foils obtained using NA and PG with a fixed pre-exponential A_s for both EOS - $A_{s,5\text{MPa}} = 1.1 \times 10^{-9} \text{ s}^{-1}$, $A_{s,7.5\text{MPa}} = 2.98 \times 10^{-9} \text{ s}^{-1}$ and $A_{s,10\text{MPa}} = 3.7 \times 10^{-9} \text{ s}^{-1}$; the co-volumes remained unchanged $b_{5\text{MPa}} = 9.38 \times 10^{-4} \text{ m}^3/\text{kg}$, $b_{7.5\text{MPa}} = 1.305 \times 10^{-3} \text{ m}^3/\text{kg}$ and $b_{10\text{MPa}} = 1.45 \times 10^{-3} \text{ m}^3/\text{kg}$. The corresponding half-reaction lengths are $l_{1/2,5\text{MPa}} = 6.71\mu\text{m}$ (PG)/ $7.65\mu\text{m}$ (NA), $l_{1/2,7.5\text{MPa}} = 2.5\mu\text{m}$ (PG)/ $3.2\mu\text{m}$ (NA) and $l_{1/2,10\text{MPa}} = 2\mu\text{m}$ (PG)/ $2.8\mu\text{m}$ (NA). As expected, the difference observed in the cellular structure comes from an effective change in the isentropic coefficient, χ_s , brought about by the volume correction made in the EOS.

This is the author's peer reviewed, accepted manuscript. However, the online version of record will be different from this version once it has been copyedited and typeset.

PLEASE CITE THIS ARTICLE AS DOI: 10.1063/5.0040723

“EOS influence on gaseous detonations”

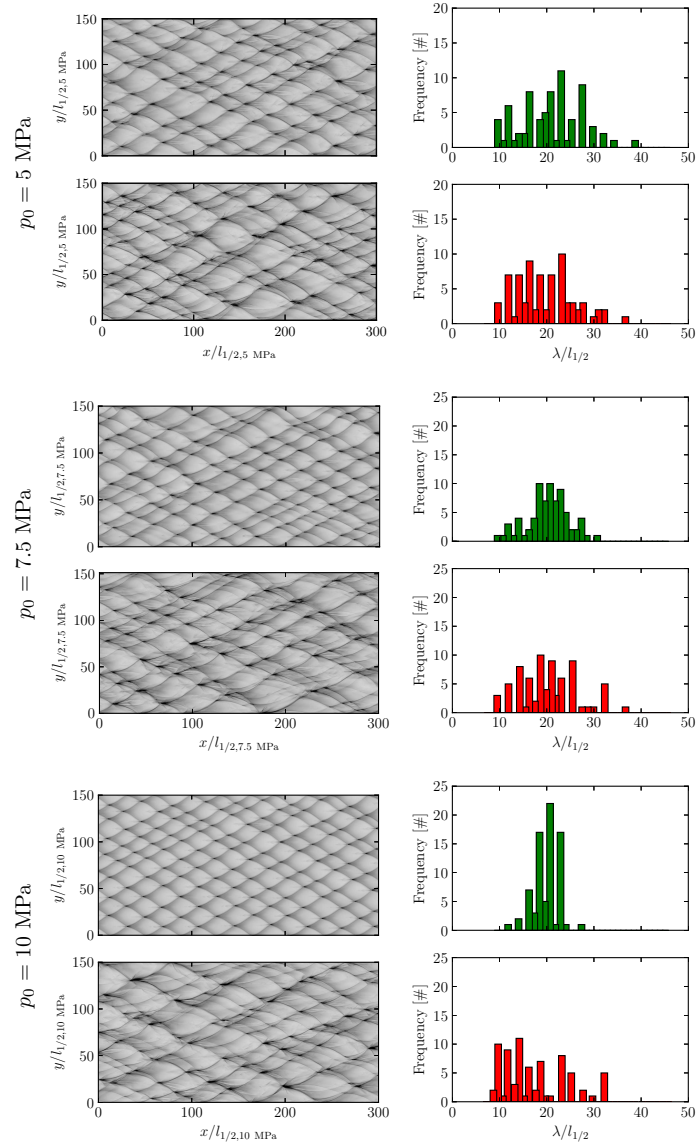
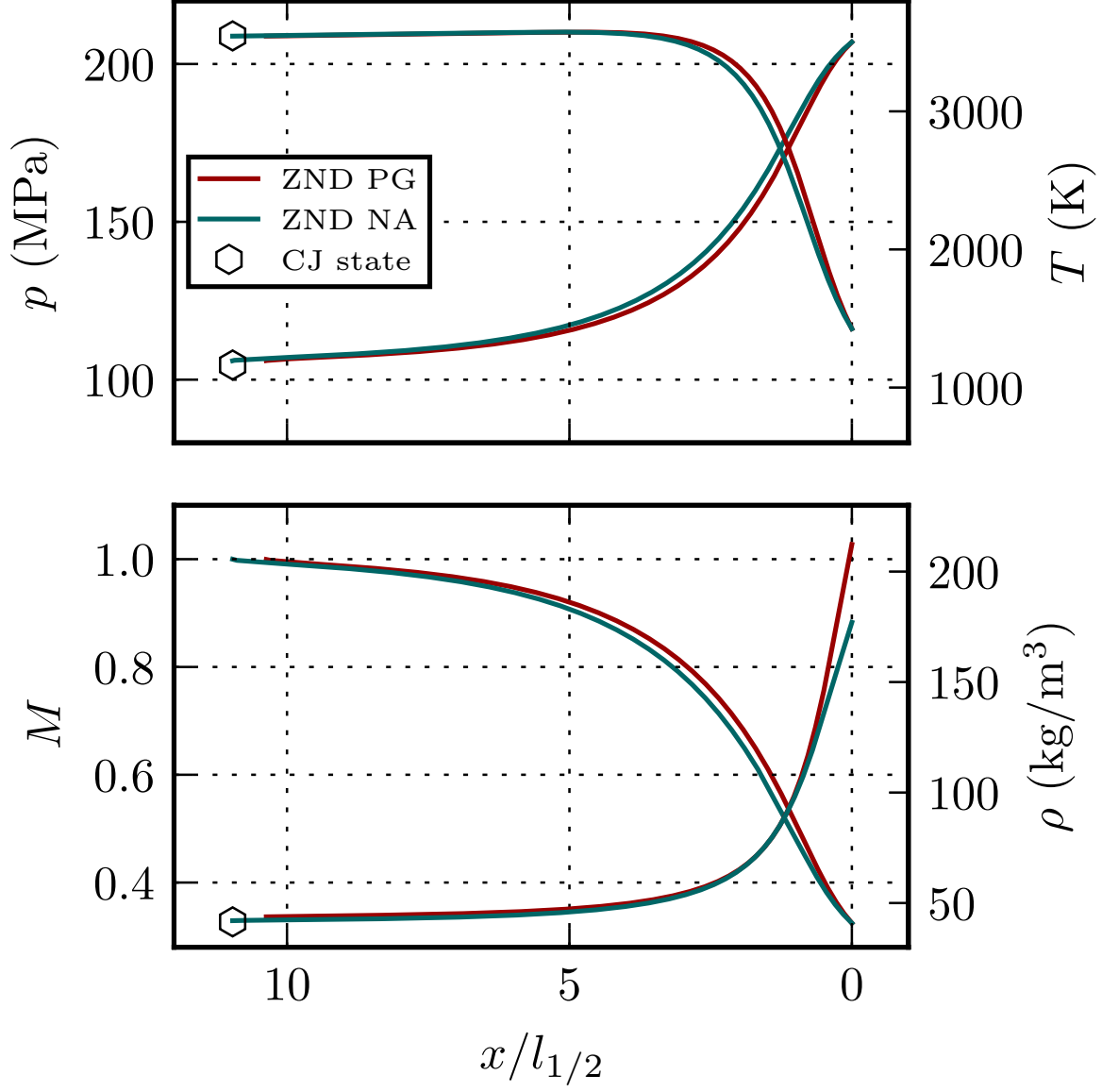


Figure 10: Numerical soot foils obtained using NA (top) and PG (bottom) for $p_0 = 5$ MPa, 7.5 MPa and 10 MPa keeping the pre-exponential factors, A_s , fixed for both EOS.

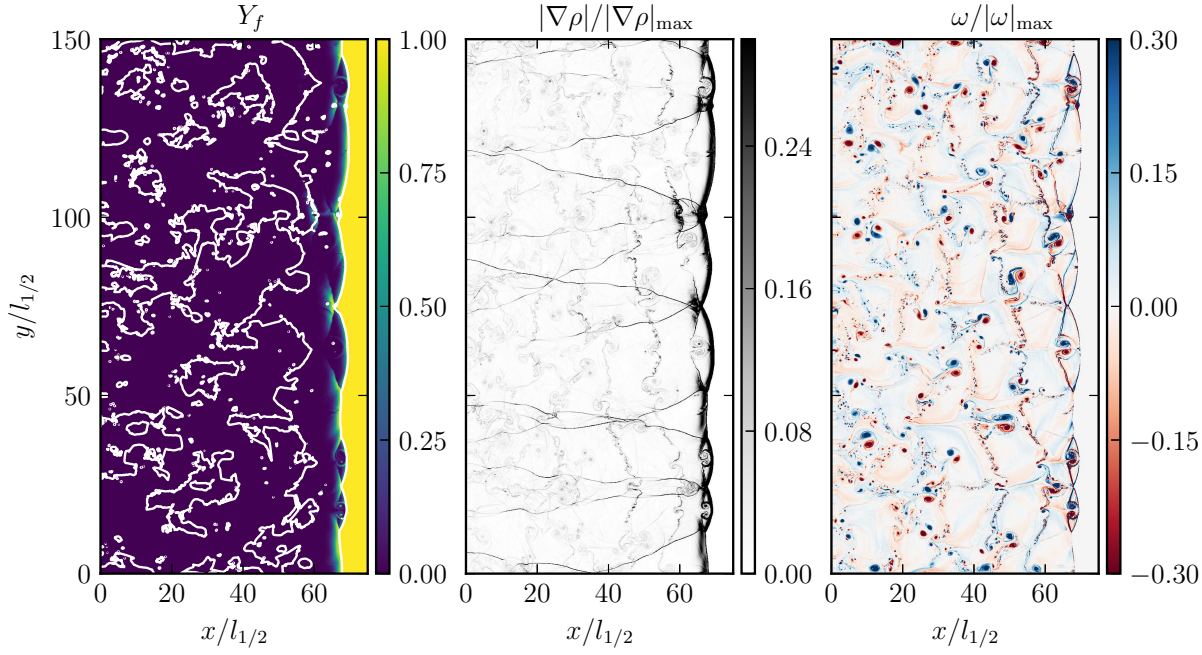
This is the author's peer reviewed, accepted manuscript. However, the online version of record will be different from this version once it has been copyedited and typeset.

PLEASE CITE THIS ARTICLE AS DOI: 10.1063/5.0040723



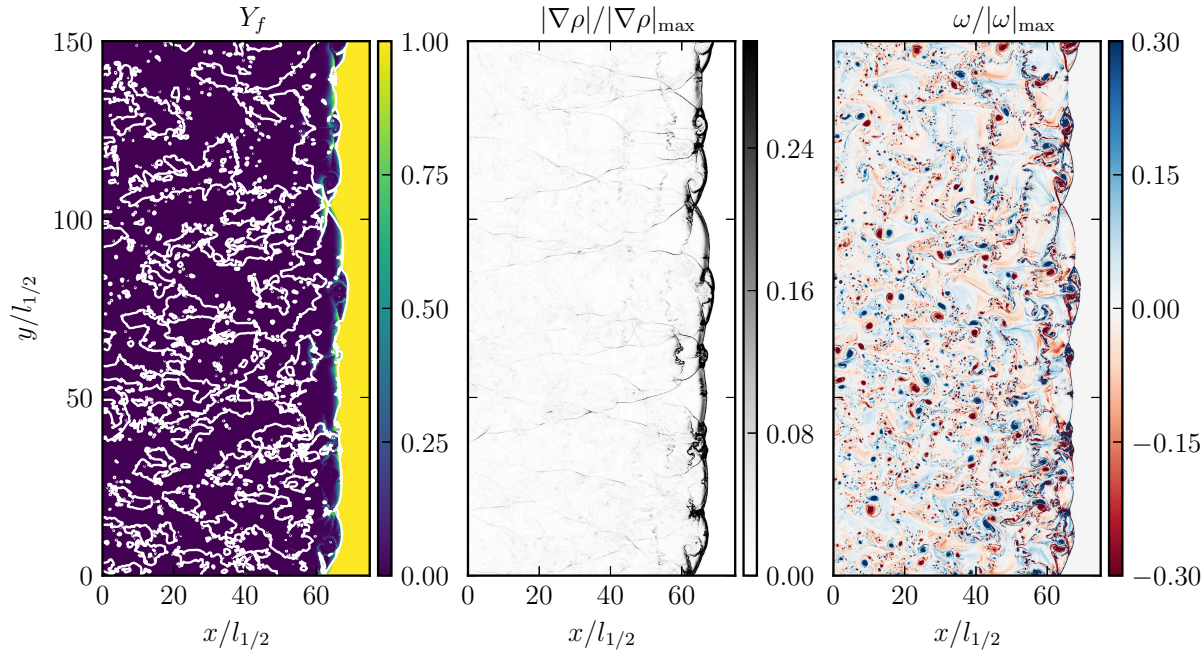
This is the author's peer reviewed, accepted manuscript. However, the online version of record will be different from this version once it has been copyedited and typeset.

PLEASE CITE THIS ARTICLE AS DOI: 10.1063/5.0040723



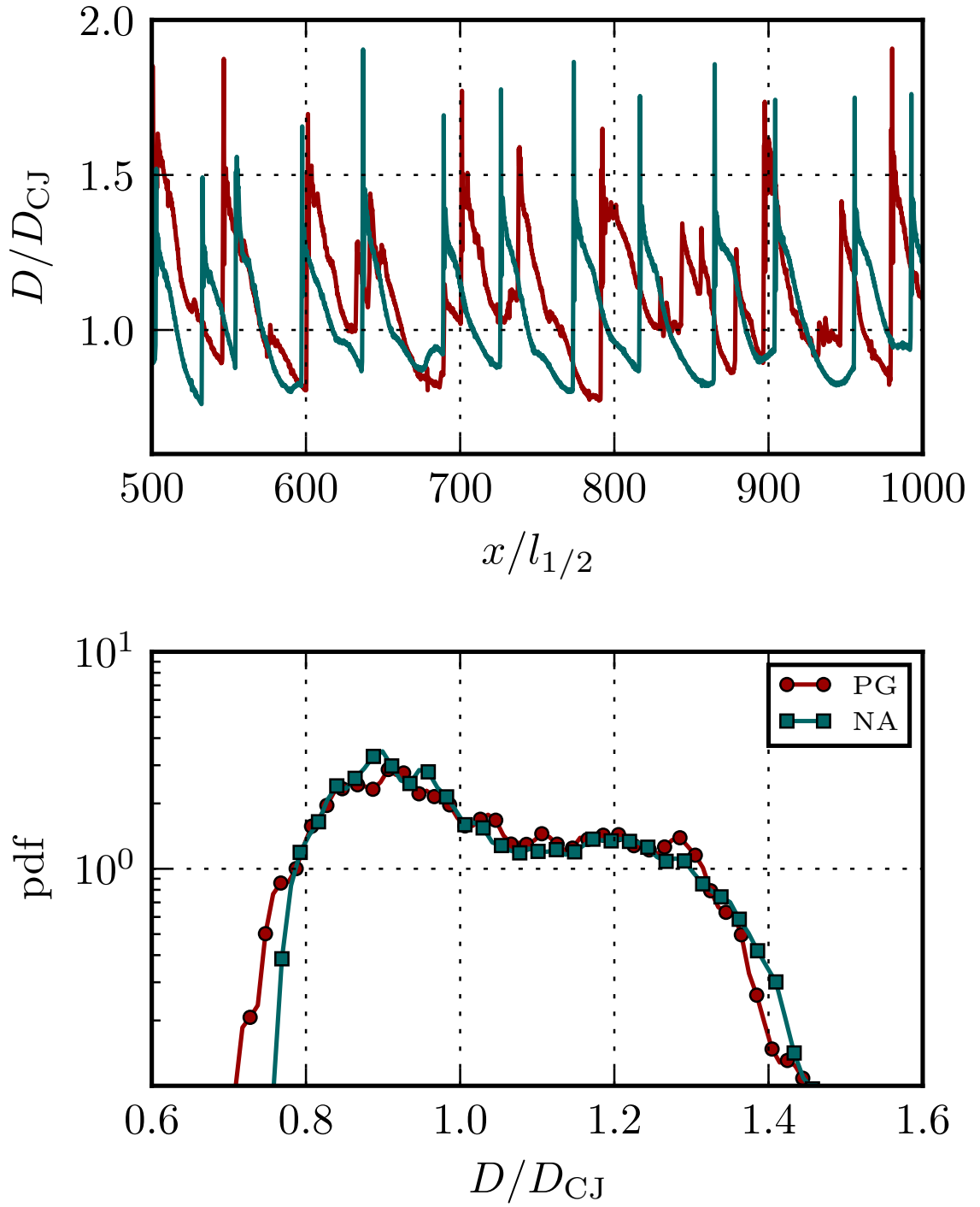
This is the author's peer reviewed, accepted manuscript. However, the online version of record will be different from this version once it has been copyedited and typeset.

PLEASE CITE THIS ARTICLE AS DOI: 10.1063/1.50040723



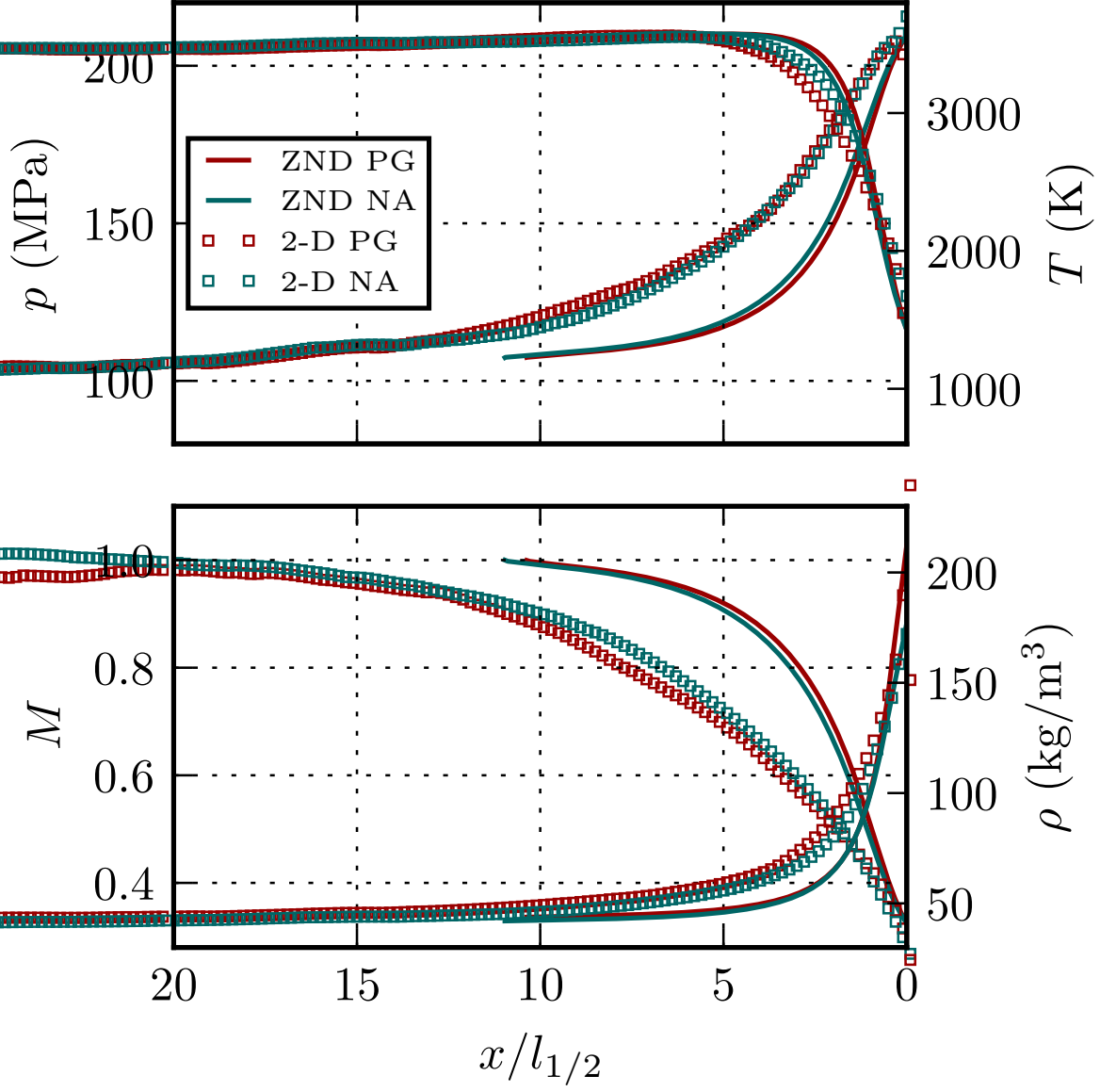
This is the author's peer reviewed, accepted manuscript. However, the online version of record will be different from this version once it has been copyedited and typeset.

PLEASE CITE THIS ARTICLE AS DOI: 10.1063/5.0040723



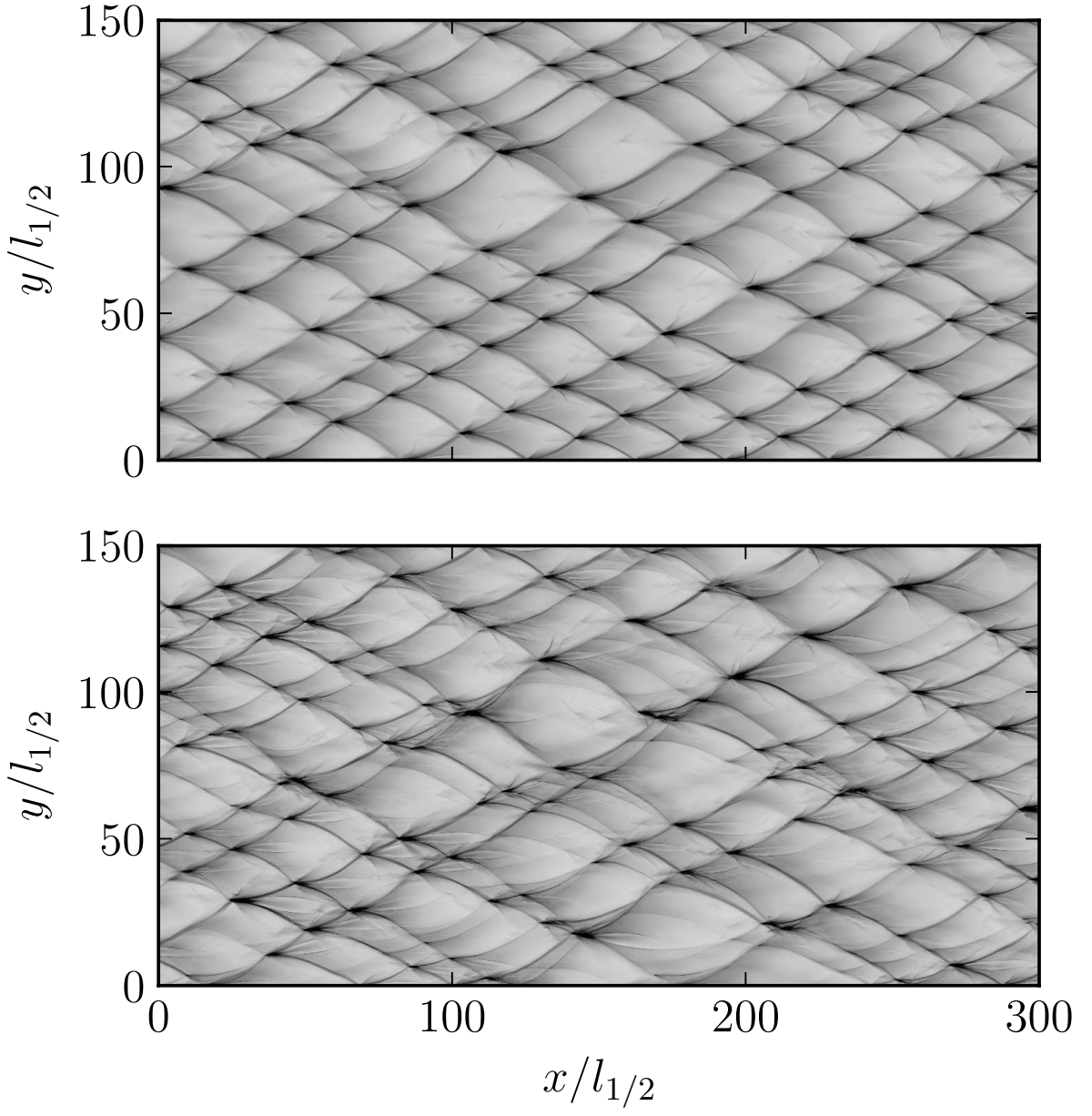
This is the author's peer reviewed, accepted manuscript. However, the online version of record will be different from this version once it has been copyedited and typeset.

PLEASE CITE THIS ARTICLE AS DOI: 10.1063/5.0040723



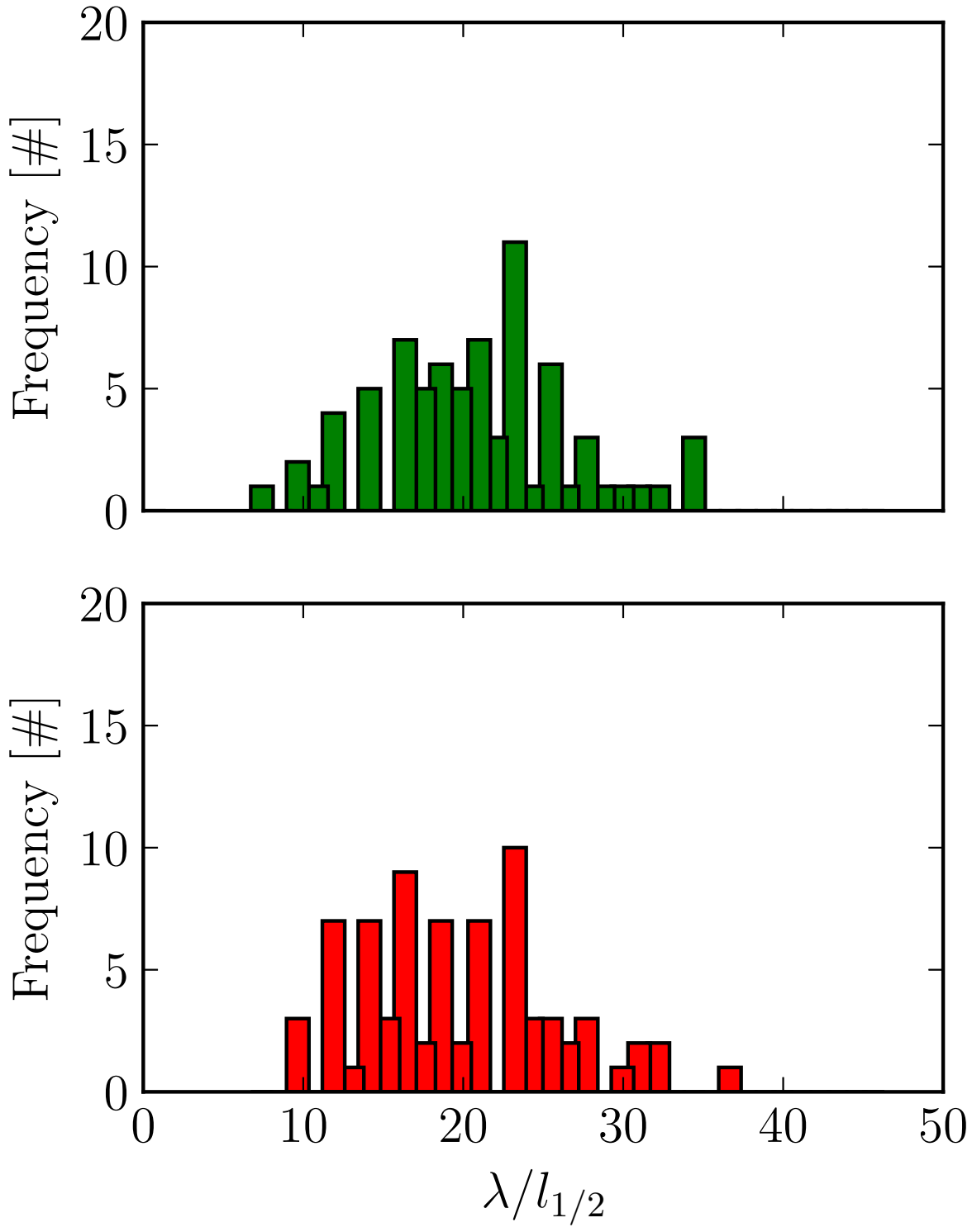
This is the author's peer reviewed, accepted manuscript. However, the online version of record will be different from this version once it has been copyedited and typeset.

PLEASE CITE THIS ARTICLE AS DOI: 10.1063/1.50040723



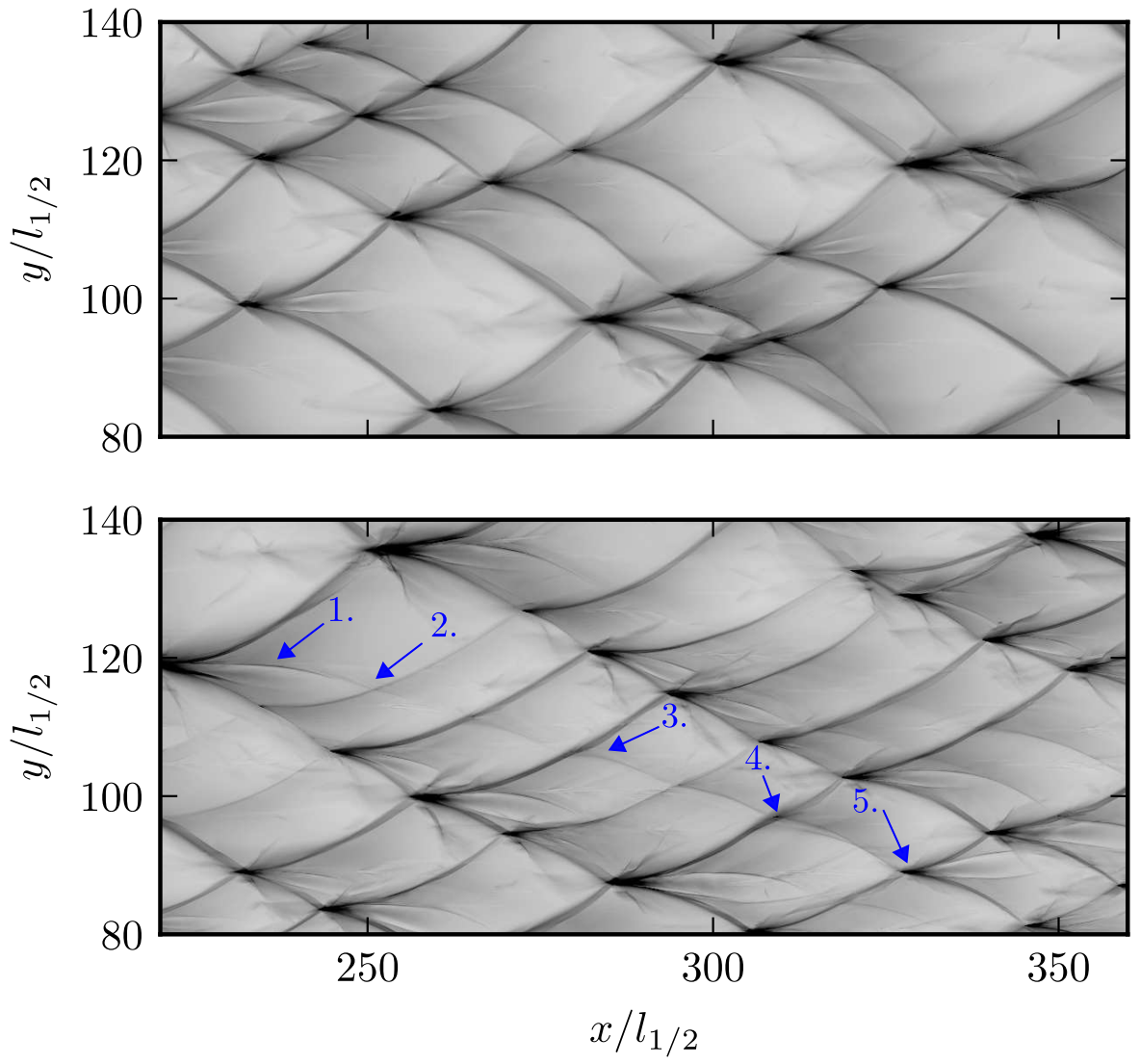
This is the author's peer reviewed, accepted manuscript. However, the online version of record will be different from this version once it has been copyedited and typeset.

PLEASE CITE THIS ARTICLE AS DOI: 10.1063/1.50040723



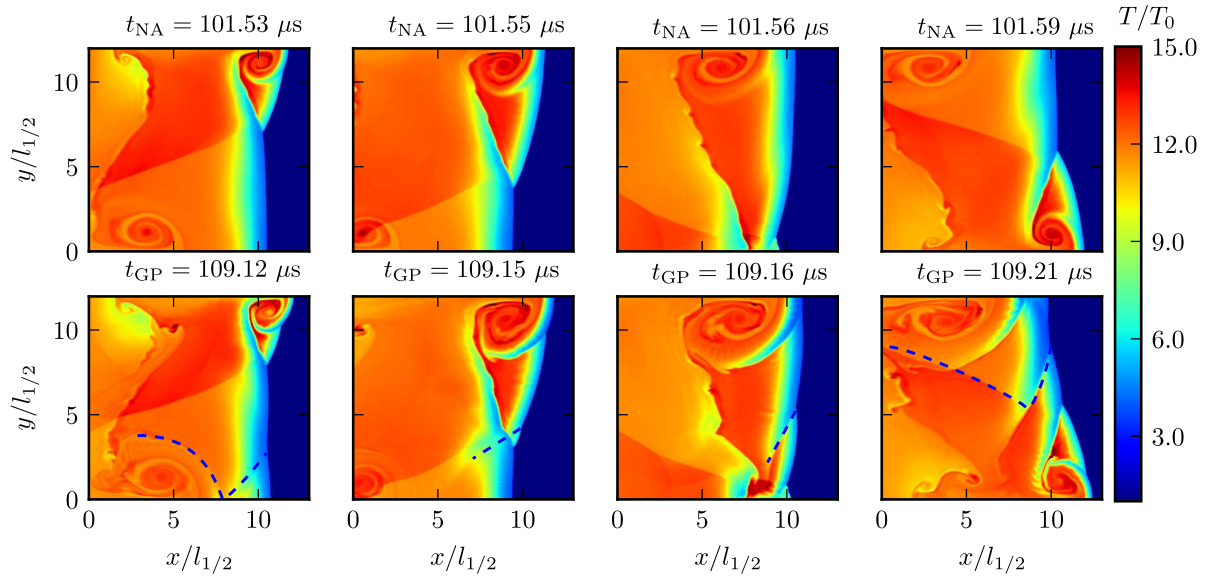
This is the author's peer reviewed, accepted manuscript. However, the online version of record will be different from this version once it has been copyedited and typeset.

PLEASE CITE THIS ARTICLE AS DOI: 10.1063/1.50040723



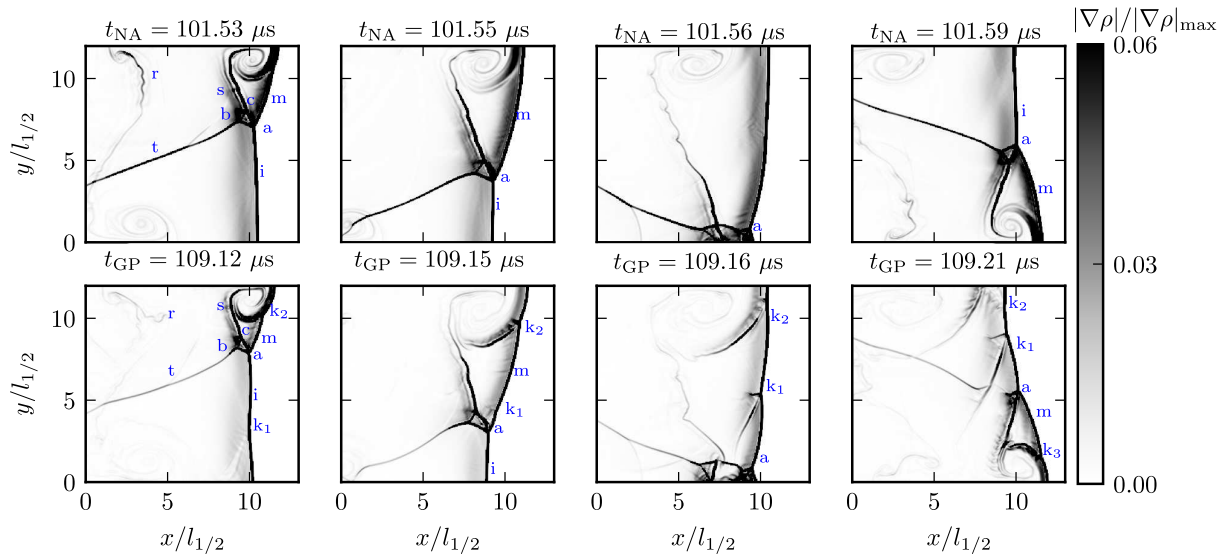
This is the author's peer reviewed, accepted manuscript. However, the online version of record will be different from this version once it has been copyedited and typeset.

PLEASE CITE THIS ARTICLE AS DOI: 10.1063/1.50040723



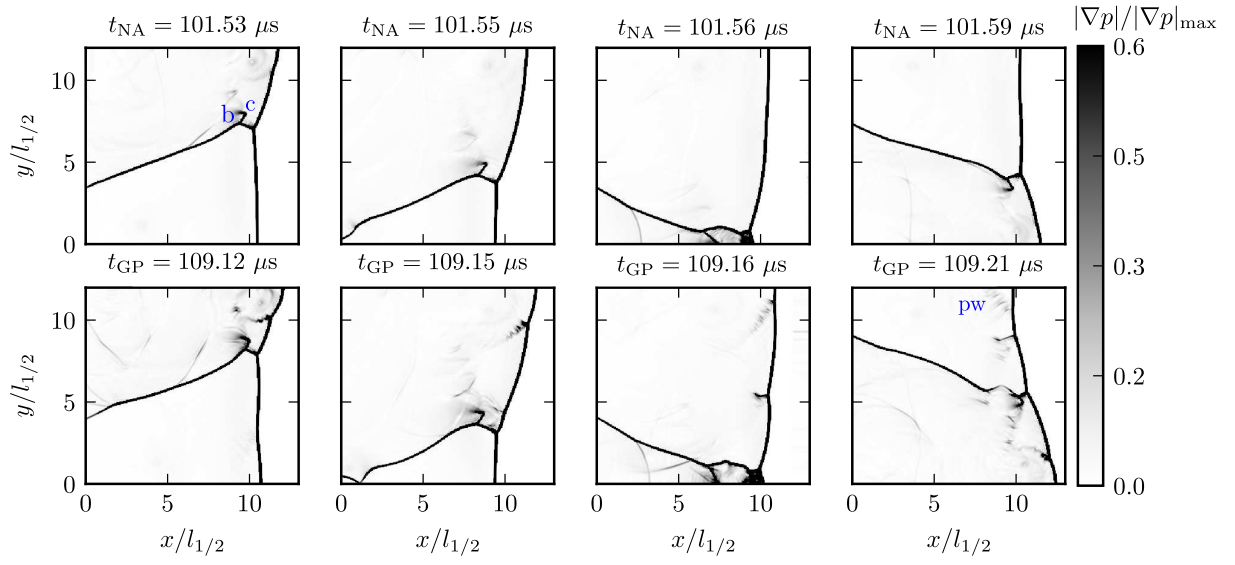
This is the author's peer reviewed, accepted manuscript. However, the online version of record will be different from this version once it has been copyedited and typeset.

PLEASE CITE THIS ARTICLE AS DOI: 10.1063/5.0040723



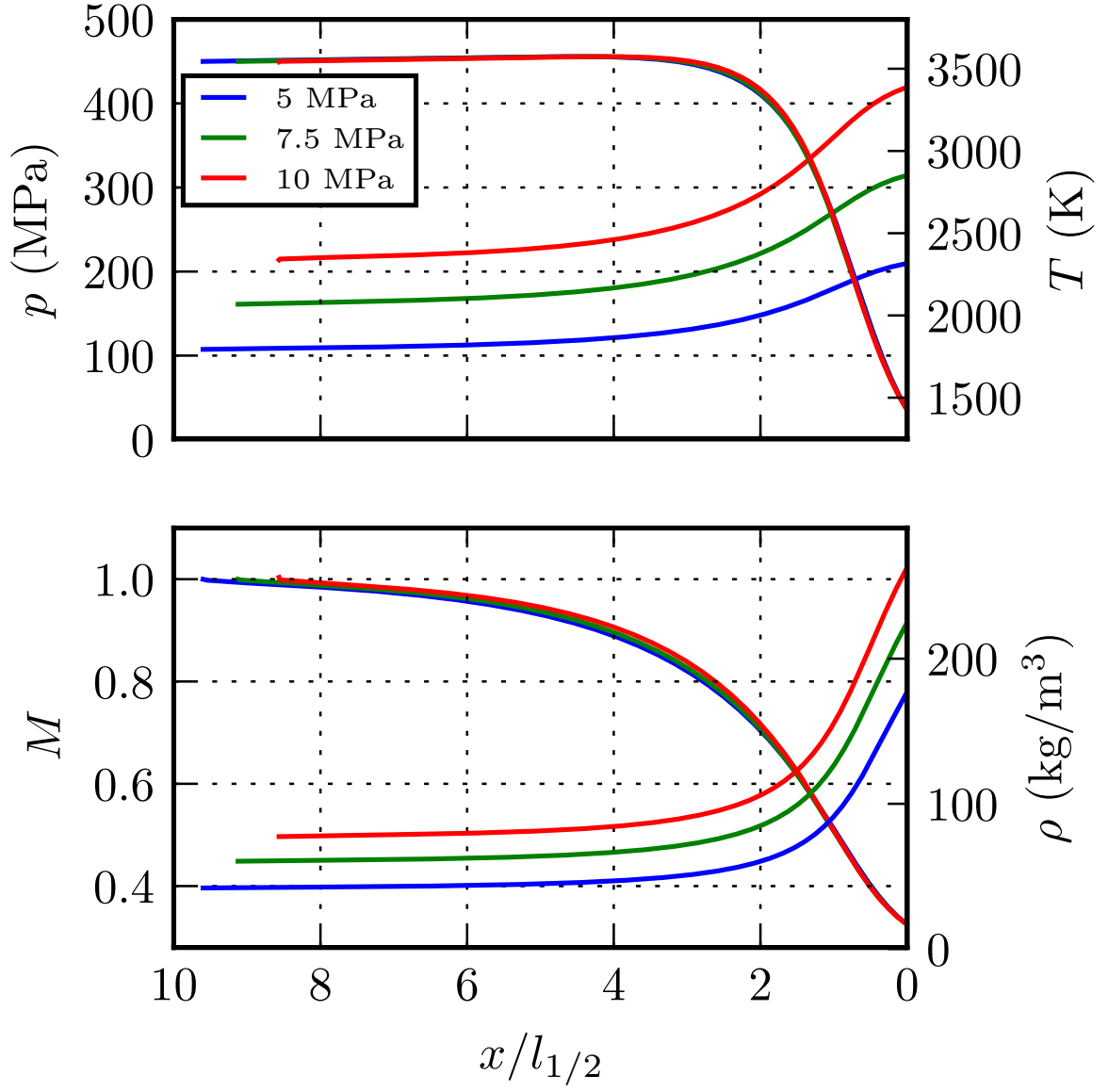
This is the author's peer reviewed, accepted manuscript. However, the online version of record will be different from this version once it has been copyedited and typeset.

PLEASE CITE THIS ARTICLE AS DOI: 10.1063/1.50040723



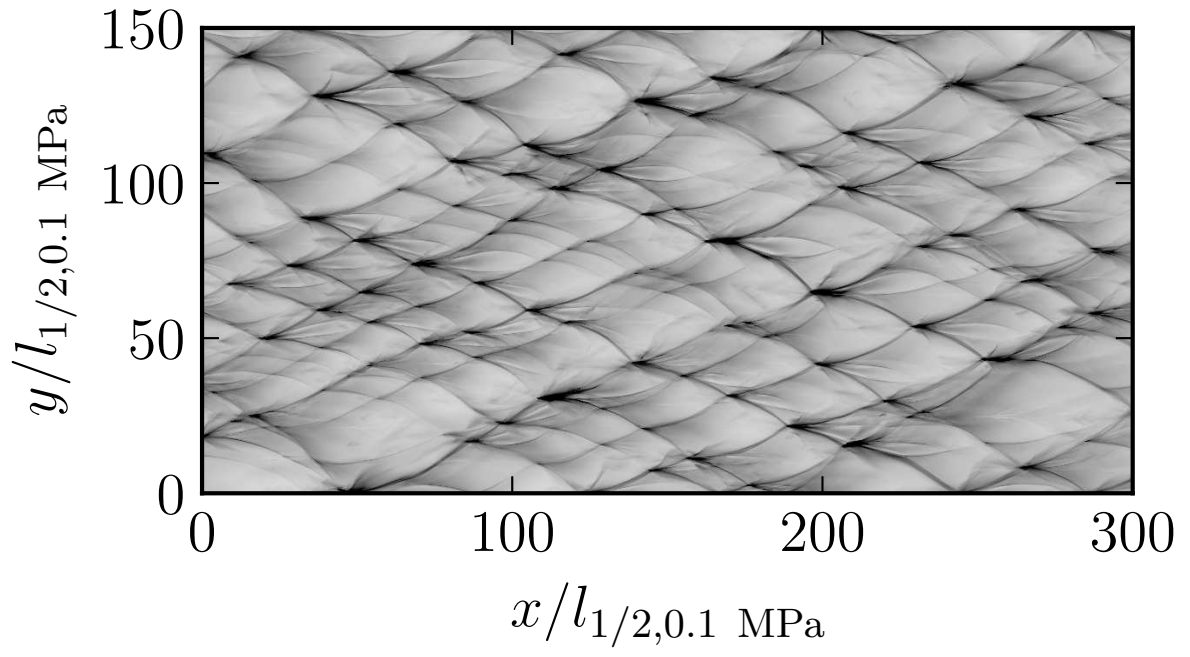
This is the author's peer reviewed, accepted manuscript. However, the online version of record will be different from this version once it has been copyedited and typeset.

PLEASE CITE THIS ARTICLE AS DOI: 10.1063/5.0040723



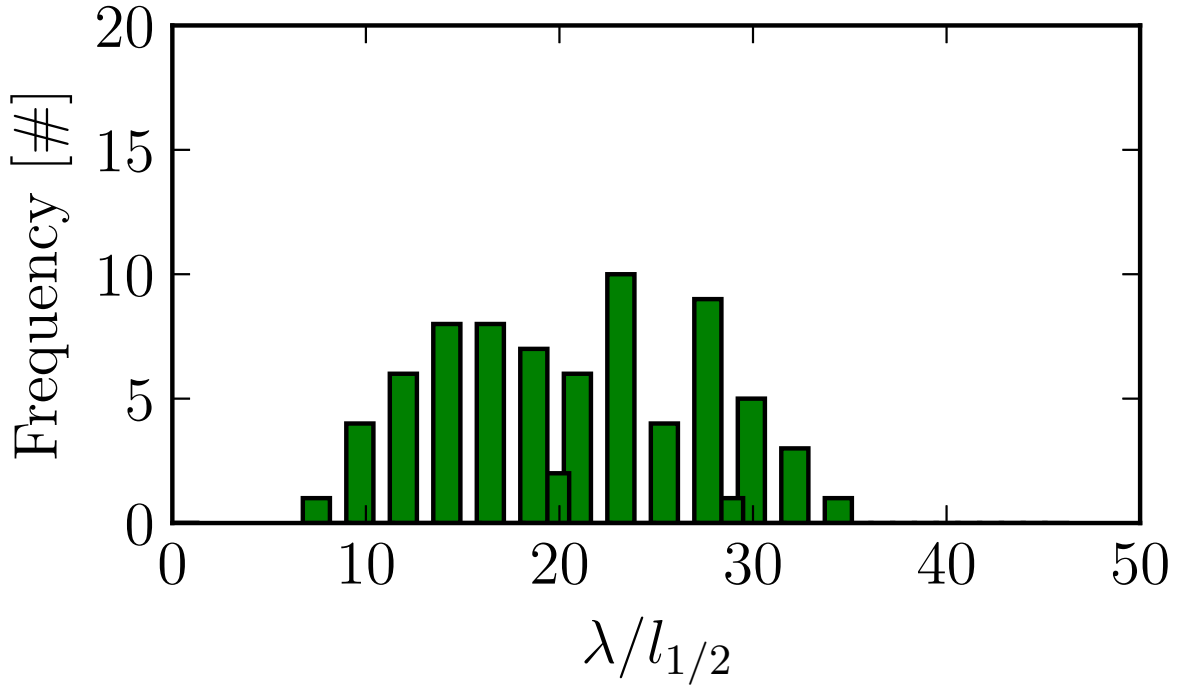
This is the author's peer reviewed, accepted manuscript. However, the online version of record will be different from this version once it has been copyedited and typeset.

PLEASE CITE THIS ARTICLE AS DOI: 10.1063/1.50040723



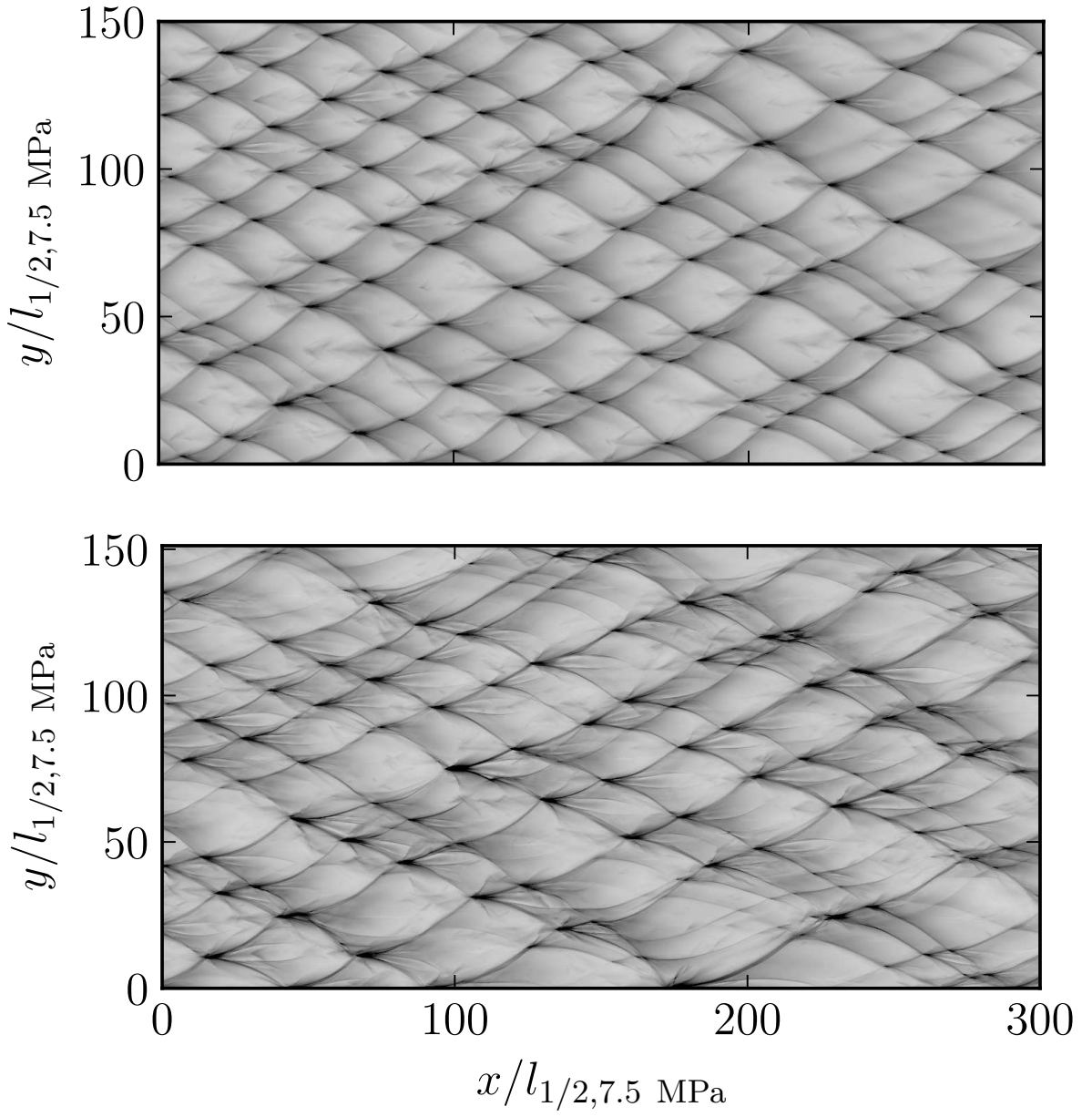
This is the author's peer reviewed, accepted manuscript. However, the online version of record will be different from this version once it has been copyedited and typeset.

PLEASE CITE THIS ARTICLE AS DOI: 10.1063/5.0040723



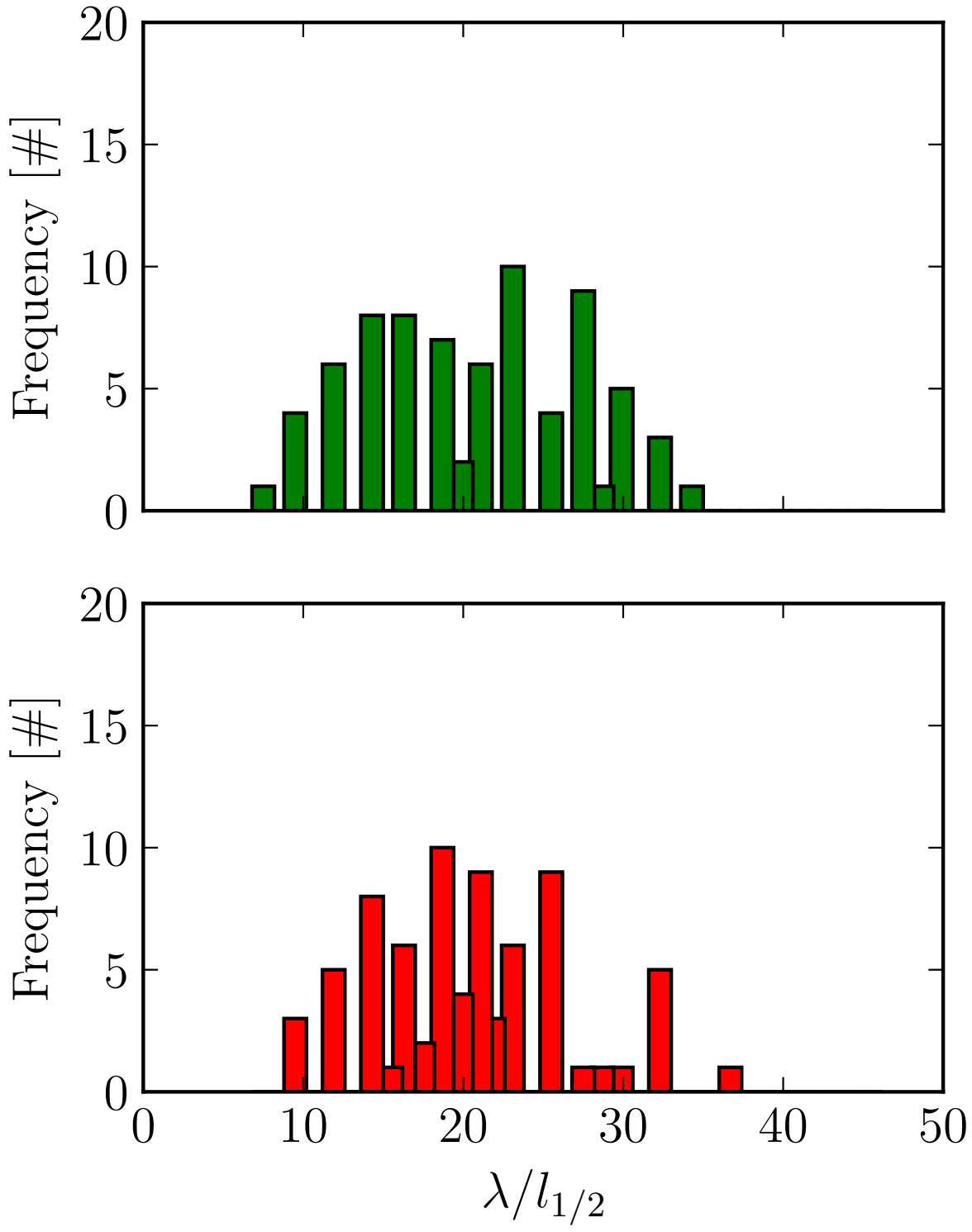
This is the author's peer reviewed, accepted manuscript. However, the online version of record will be different from this version once it has been copyedited and typeset.

PLEASE CITE THIS ARTICLE AS DOI: 10.1063/1.50040723



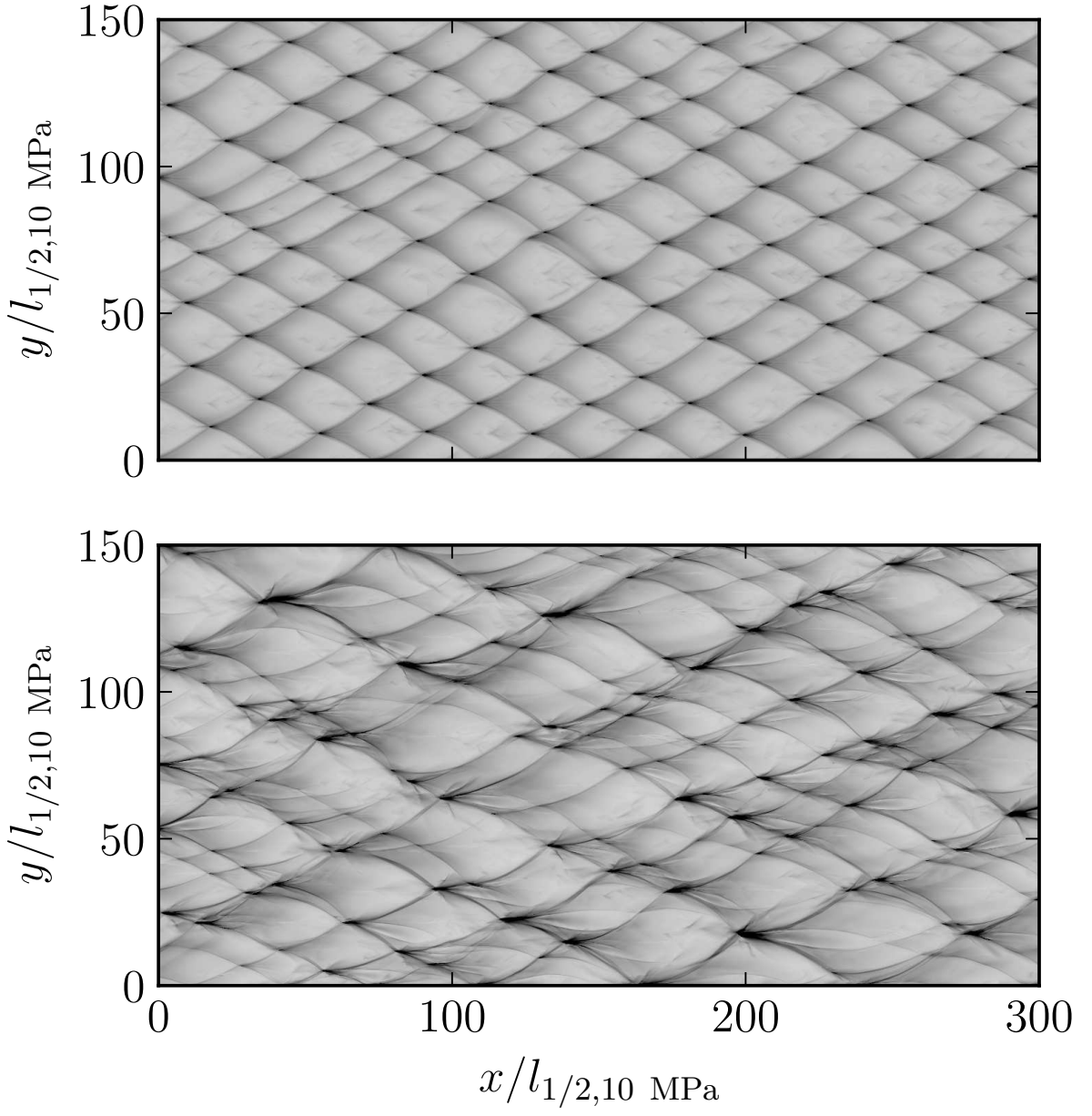
This is the author's peer reviewed, accepted manuscript. However, the online version of record will be different from this version once it has been copyedited and typeset.

PLEASE CITE THIS ARTICLE AS DOI: 10.1063/5.0040723



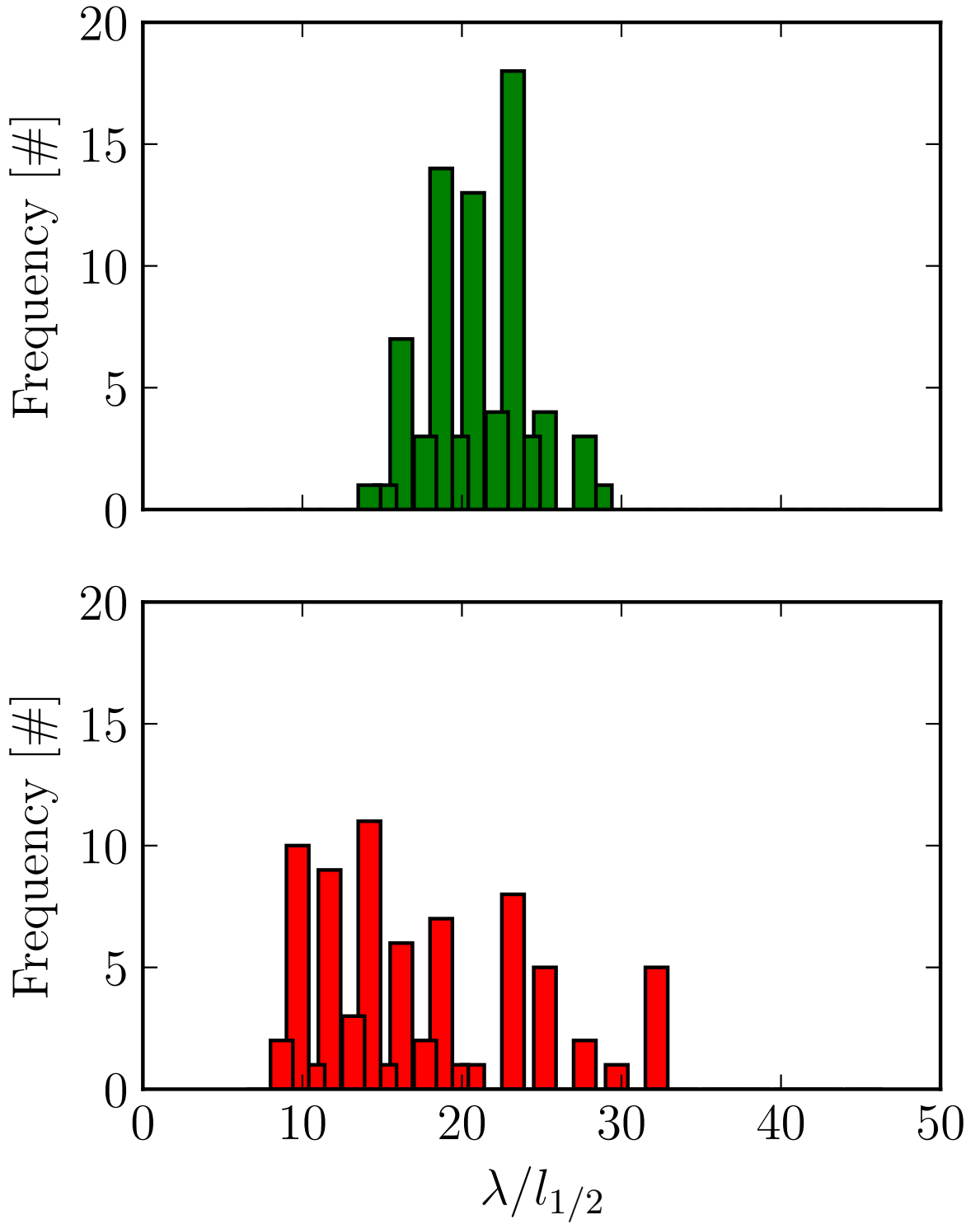
This is the author's peer reviewed, accepted manuscript. However, the online version of record will be different from this version once it has been copyedited and typeset.

PLEASE CITE THIS ARTICLE AS DOI: 10.1063/1.50040723



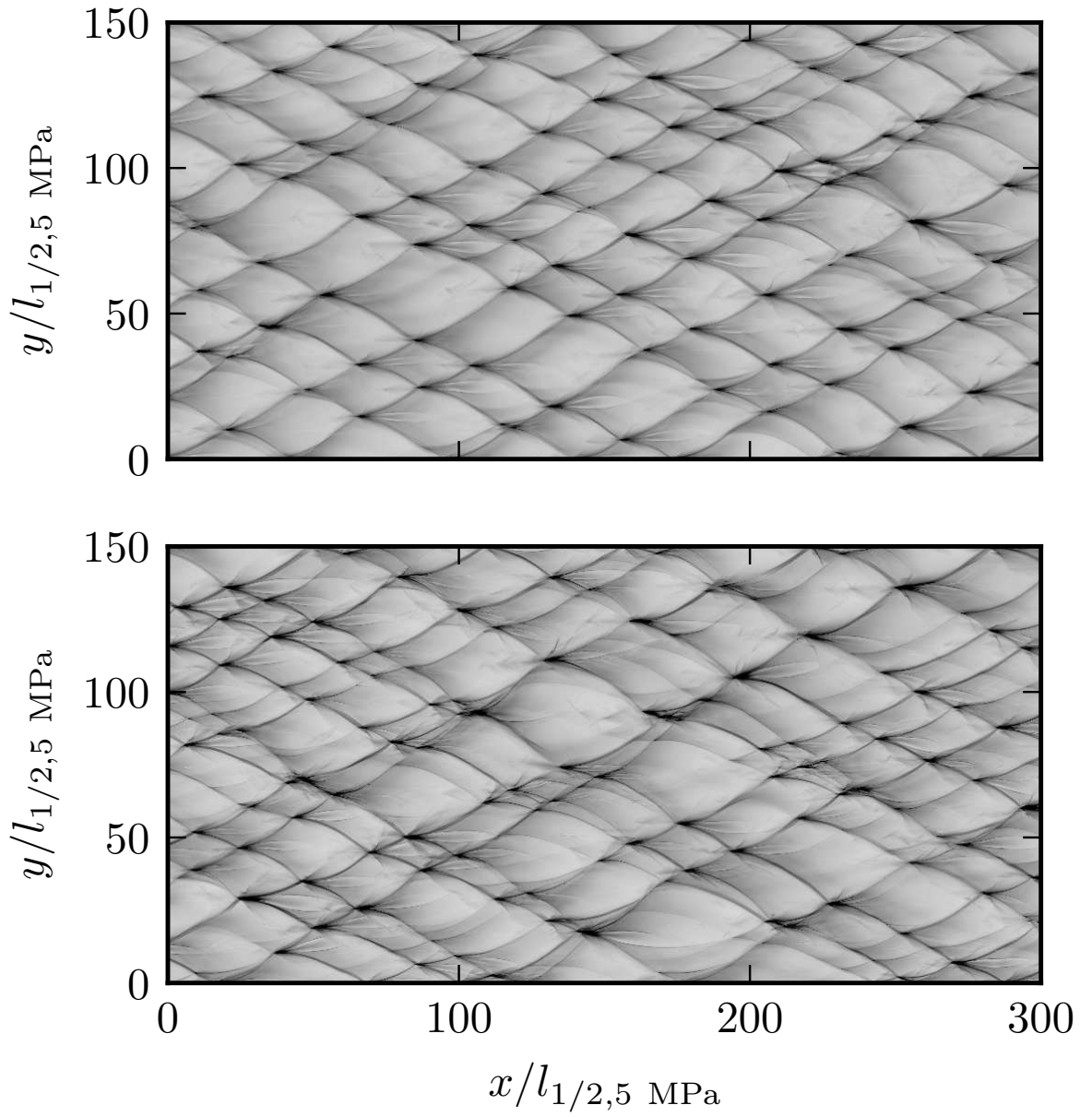
This is the author's peer reviewed, accepted manuscript. However, the online version of record will be different from this version once it has been copyedited and typeset.

PLEASE CITE THIS ARTICLE AS DOI: 10.1063/5.0040723



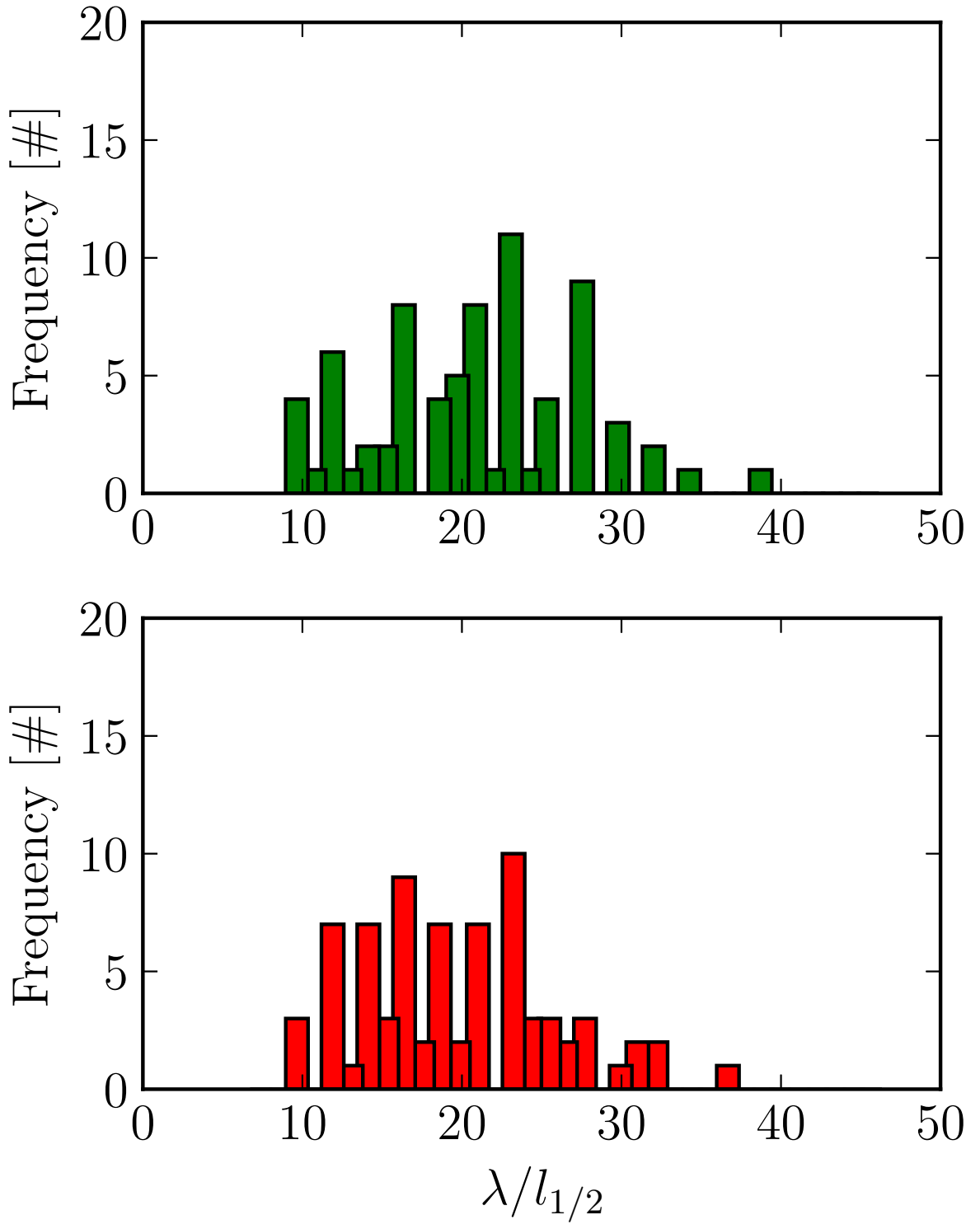
This is the author's peer reviewed, accepted manuscript. However, the online version of record will be different from this version once it has been copyedited and typeset.

PLEASE CITE THIS ARTICLE AS DOI: 10.1063/1.50040723



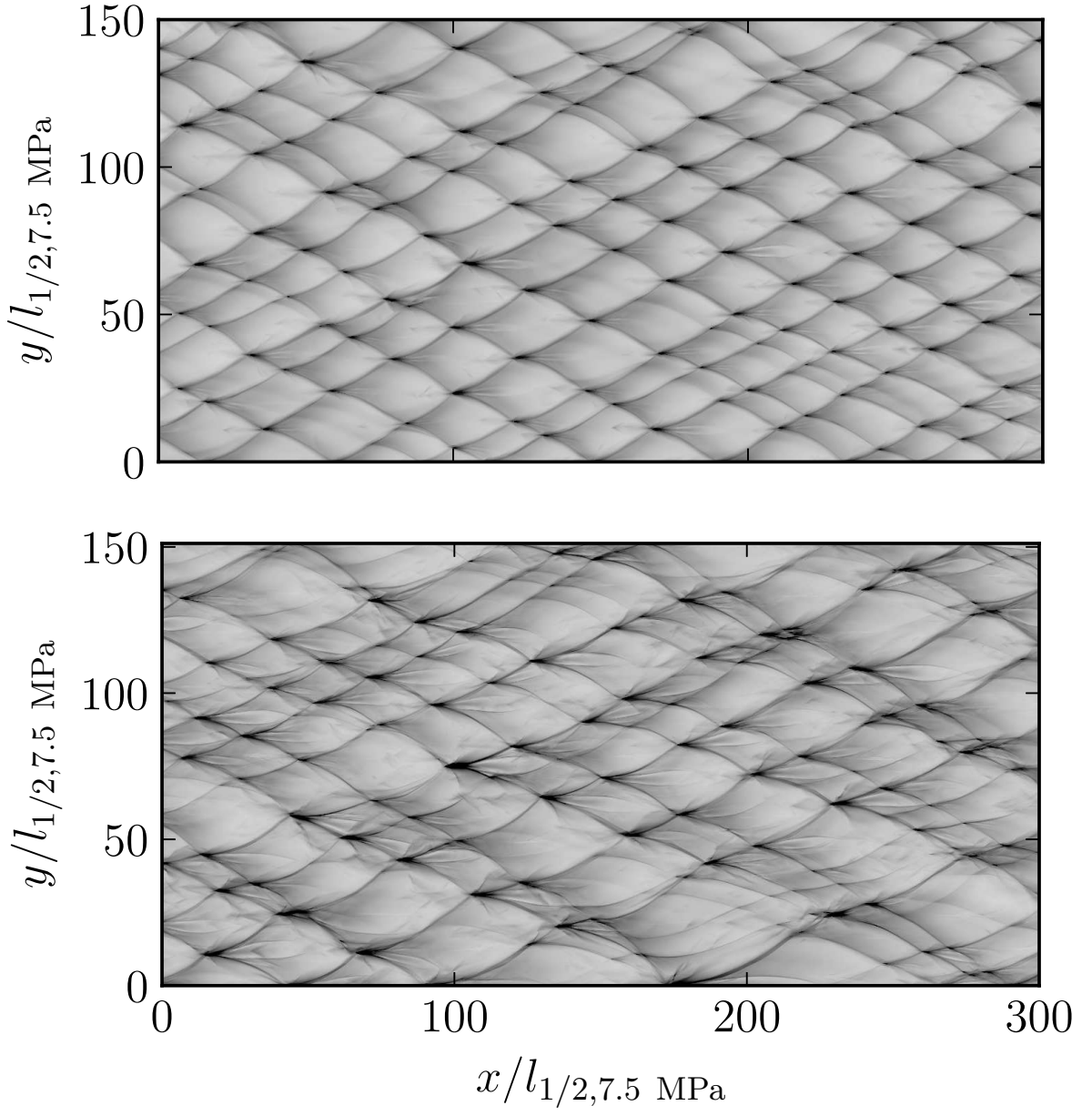
This is the author's peer reviewed, accepted manuscript. However, the online version of record will be different from this version once it has been copyedited and typeset.

PLEASE CITE THIS ARTICLE AS DOI: 10.1063/5.0040723



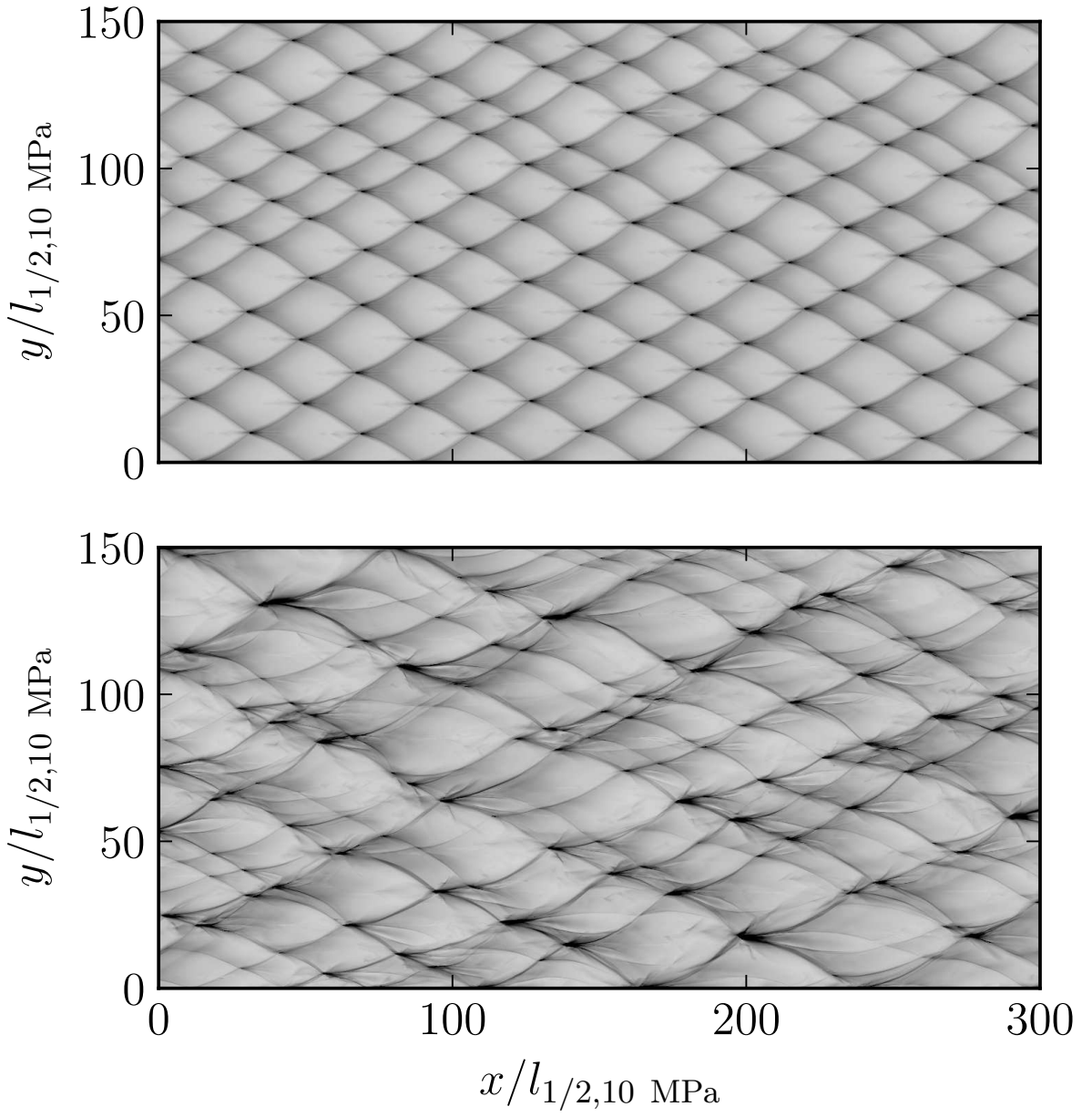
This is the author's peer reviewed, accepted manuscript. However, the online version of record will be different from this version once it has been copyedited and typeset.

PLEASE CITE THIS ARTICLE AS DOI: 10.1063/1.50040723



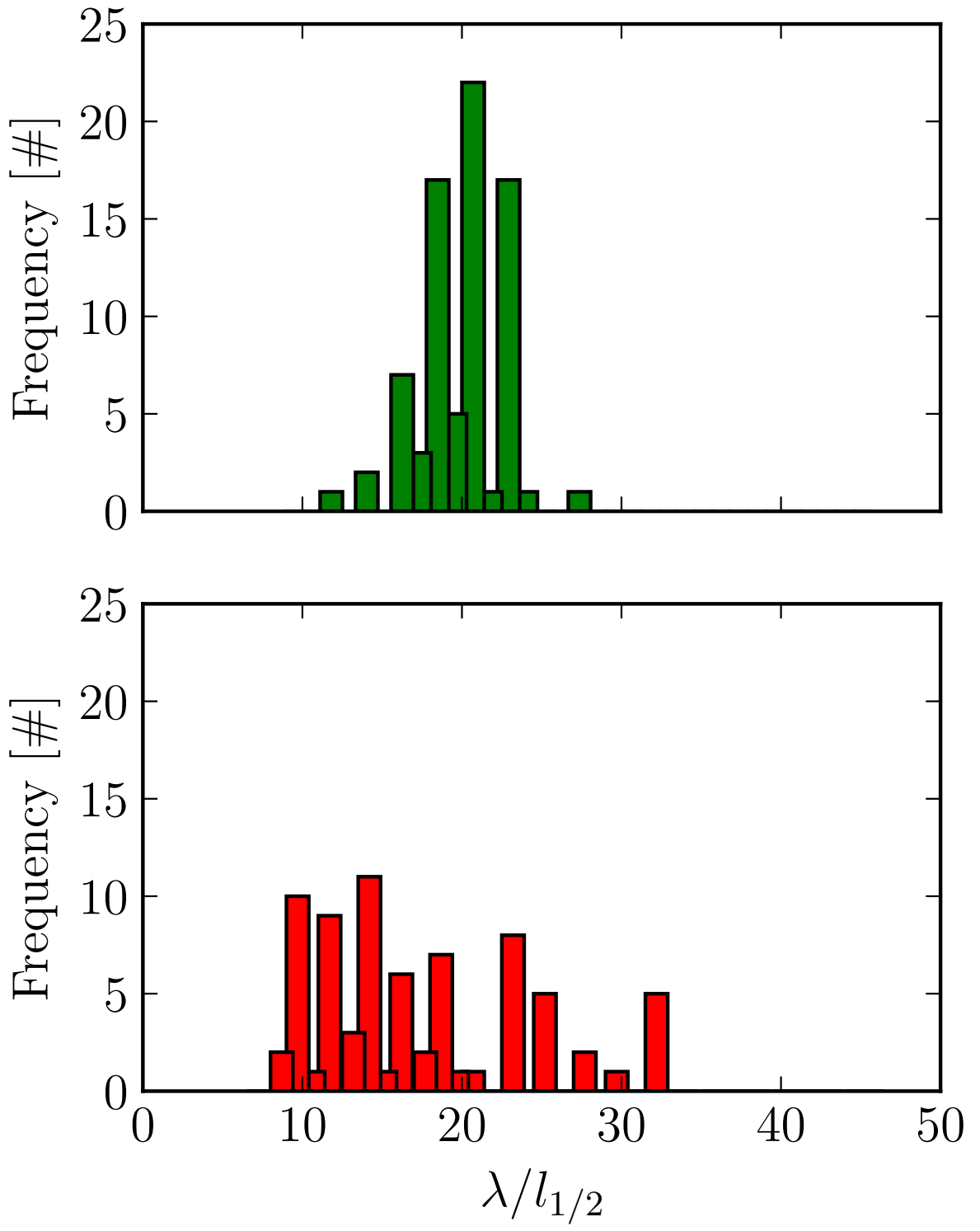
This is the author's peer reviewed, accepted manuscript. However, the online version of record will be different from this version once it has been copyedited and typeset.

PLEASE CITE THIS ARTICLE AS DOI: 10.1063/1.50040723



This is the author's peer reviewed, accepted manuscript. However, the online version of record will be different from this version once it has been copyedited and typeset.

PLEASE CITE THIS ARTICLE AS DOI: 10.1063/5.0040723



This is the author's peer reviewed, accepted manuscript. However, the online version of record will be different from this version once it has been copyedited and typeset.

PLEASE CITE THIS ARTICLE AS DOI: 10.1063/5.0040723

